PFG

Photogrammetrie Fernerkundung Geoinformation

Journal for Photogrammetry, Remote Sensing and Geoinformation Science

Organ der Deutschen Gesellschaft für Photogrammetrie, Fernerkundung und Geoinformation (DGPF) e. V.

Jahrgang 2015, Heft 6

E. Schweizerbart'sche Verlagsbuchhandlung
(Nägele u. Obermiller) Stuttgart 2015

Deutsche Gesellschaft für Photogrammetrie, Fernerkundung
und Geoinformation (DGPF) e. V.
Gegründet 1909

Die *Deutsche Gesellschaft für Photogrammetrie, Fernerkundung und Geoinformation* (DGPF) e. V. unterstützt als Mitglieds- bzw. Trägergesellschaft die folgenden Dachverbände:

International Society
for Photogrammetry
and Remote Sensing

DAGM

Deutsche Arbeits-
gemeinschaft für
Mustererkennung e.V.

GeoUnion
Alfred-Wegener-Stiftung

Herausgeber:

Präsident: Prof. Dr. Thomas Kolbe, Technische Universität München, Institut für Geodäsie, GIS und Landmanagement, Lehrstuhl für Geoinformatik, Arcisstraße 21, 80333 München, Germany, Tel. +49-89-289-23888
Geschäftsstelle: Tanja Nyc, c/o Technische Universität München, Institut für Geodäsie, GIS und Landmanagement, Lehrstuhl für Geoinformatik, Arcisstraße 21, 80333 München, Germany, Tel.: +49-89-289-22578, e-mail: geschaeftsstelle@dgpf.de
Published by: E. Schweizerbart'sche Verlagsbuchhandlung (Nägele u. Obermiller), Johannesstraße 3A, 70176 Stuttgart, Germany, Tel.: +49-711 351456-0, Fax: +49-711 351456-99, e-mail: mail@schweizerbart.de
Internet: http://www.schweizerbart.de
⊘ Gedruckt auf alterungsbeständigem Papier nach ISO 9706-1994

ISSN 1432-8364 / e-ISSN 2363-7145
Science Citation Index Expanded (also known as SciSearch®) Journal Citation Reports/Science Edition
Hauptschriftleiter: Prof. Dr.-Ing. Wolfgang Kresse, Hochschule Neubrandenburg, Fachbereich Landschaftswissenschaften und Geomatik, Brodaer Straße 2, 17033 Neubrandenburg, Germany, e-mail: kresse@hs-nb.de
Schriftleiter: Prof. Dr.-Ing. Stefan Hinz, Karlsruher Institut für Technologie – KIT, Institut für Photogrammetrie und Fernerkundung, Englerstraße 7, 76131 Karlsruhe, Germany, e-mail: stefan.hinz@ipf.uni-karlsruhe.de, Prof. Dr. techn. Franz Rottensteiner, Leibniz Universität Hannover, Institut für Photogrammetrie und GeoInformation, Nienburger Straße 1, 30167 Hannover, Germany, e-mail: rottensteiner@ipi.uni-hannover.de, Prof. Dr. rer. nat. Christopher Conrad, Universität Würzburg, Institut für Geographie und Geologie, Oswald-Külpe-Weg 86, 97074 Würzburg, Germany, e-mail: christopher.conrad@uni-wuerzburg.de, Prof. Dr. rer. nat. Lars Bernard, Technische Universität Dresden, Fachrichtung Geowissenschaften, Helmholtzstraße 10, 01062 Dresden, Germany, e-mail: lars.bernard@tu-dresden.de, und Dr.-Ing. Eckhardt Seyfert, Landesvermessung und Geobasisinformation Brandenburg, Heinrich-Mann-Allee 103, 14473 Potsdam, Germany, e-mail: eckhardt.seyfert@geobasis-bb.de
Erscheinungsweise: 6 Hefte pro Jahrgang.
Bezugspreis im Abonnement: € 249,– pro Jahrgang. Mitglieder der DGPF erhalten die Zeitschrift kostenlos. Der Online-Zugang ist im regulären Subskriptionspreis enthalten.
Anzeigenverwaltung: E. Schweizerbart'sche Verlagsbuchhandlung (Nägele u. Obermiller), Johannesstraße 3A, 70176 Stuttgart, Germany, Tel.: +49-711 351456-0; Fax: +49-711 351456-99.
e-mail: mail@schweizerbart.de, Internet: http://www.schweizerbart.de
Bernhard Harzer Verlag GmbH, Westmarkstraße 59/59a, 76227 Karlsruhe, Germany, Tel.: +49-721 944020, Fax: +49-721 9440230, e-mail: Info@harzer.de, Internet: www.harzer.de
Printed in Germany by Tutte Druckerei & Verlagsservice GmbH, 94121 Salzweg, Germany.

PFG – Jahrgang 2015, Heft 6
Inhaltsverzeichnis

Originalbeiträge

Beitrag aus Wissenschaft und Praxis

Mitteilungen

Zusammenfassungen der „Originalbeiträge“ und der „Beiträge aus Wissenschaft und Praxis“ (deutsch und englisch) sind auch verfügbar unter www.dgpf.de/neu/pfg/ausgaben.htm

PFG 2015 / 12, 0423–0436
Stuttgart, December 2015

Article

VNIR/SWIR Laboratory Imaging Spectroscopy for Wall-to-Wall Mapping of Elemental Concentrations in Soil Cores

Simon Schreiner, Henning Buddenbaum, Christoph Emmerling, Trier & Markus Steffens, Freising

Keywords: PLSR, VNIR, SWIR, hyperspectral, soil profiles

Summary: Visible/near infrared (VNIR, 400 nm to 1000 nm wavelength) and shortwave infrared (SWIR, 1000 nm to 2500 nm wavelength) laboratory imaging spectroscopy with spatial resolutions of 63 µm and 250 µm, respectively, was used for mapping contents of C, N, Fe, Al, and Ca in soil profiles. Four soil cores of 30 cm to 50 cm length were collected at a Regosol and a Cambisol site and scanned hyperspectrally after drying. Small samples (ROI; Regions of Interest) were taken from the cores and analysed chemically as references for regression analyses. Partial least-squares regression (PLSR) and multivariate adaptive regression splines (MARS) models between spectral information and elemental contents of reference samples were established for VNIR and SWIR data separately and for the combined datasets. The regression models were applied to the hyperspectral image data to create spatially explicit maps of elemental contents for the soil profiles. PLSR yielded slightly better regression accuracies than MARS, and PLSR maps were more plausible in visual inspection. The optimal spectral range for elemental mapping was inconsistent, but in most cases the addition of SWIR data to VNIR data resulted in improvements of the elemental content estimations.

Zusammenfassung: *Abbildende Laborspektroskopie im VNIR/SWIR-Bereich zur flächendeckenden Kartierung von Elementkonzentrationen in Bodenprofilen*. Hyperspektrale Laboraufnahmen in den Wellenlängenbereichen Sichtbar/Nahinfrarot (VNIR, 400 nm bis 1000 nm Wellenlänge) und Kurzwelleninfrarot (SWIR, 1000 nm bis 2500 nm) mit räumlichen Auflösungen von 63 µm und 250 µm wurden verwendet, um die räumlichen Verteilungen von C, N, Fe, Al und Ca in Bodenprofilen zu kartieren. Vier Bodenkerne mit 30 cm bis 50 cm Länge wurden an einem Cambisol- und einem Regosol-Standort entnommen und im Labor hyperspektral abgetastet. Kleine Proben wurden aus den Profilen entnommen und als Referenz für die nachfolgenden Regressionsanalysen chemisch analysiert. Regressionsmodelle wurden mittels Partial Least-Squares Regression (PLSR) und Multivariate Adaptive Regression Splines (MARS) zwischen Spektralinformationen und Elementkonzentrationen der Referenzproben aufgestellt, separat für VNIR- und SWIR-Daten und für die kombinierten Datensätze. Die Regressionsmodelle wurden auf die Bilddatensätze angewendet, um Karten der Elementkonzentrationen in den Bodenprofilen zu erzeugen. Die Regressionsgenauigkeiten von PLSR waren leicht höher als die von MARS, und die PLSR-Karten gaben einen visuell plausibleren Eindruck. Der optimale Spektralbereich zur Kartierung der verschiedenen Elemente war uneinheitlich. Aber meistens brachte die Berücksichtigung der SWIR-Daten eine Verbesserung gegenüber den VNIR-Daten alleine.

1 Introduction

Visible/near infrared (VNIR, 400 nm to 1000 nm wavelength) and shortwave infrared (SWIR, 1000 nm to 2500 nm wavelength) diffuse reflectance spectroscopy has proven to be useful for many soil scientific topics. Reflectance spectroscopy has been used in many studies for the determination of soil properties like mineral composition (Viscarra Ros-

www.schweizerbart.de
DOI: 10.1127/pfg/2015/0279
1432-8364/15/0279 $ 0.00

sel et al. 2009), texture (Stenberg 2010), biological properties (Heinze et al. 2013), soil salinity (Farifteh et al. 2008), or chemical composition (Vohland et al. 2009). The papers by Viscarra Rossel et al. (2006), Ben-Dor et al. (2009), Stenberg (2010) and Hartemink & Minasny (2014), among many others, give an overview on techniques and results of reflectance spectroscopy in soil science.

In most studies, reflectance spectroscopy was either used on samples from selected points (field and laboratory spectroscopy), or on the soil surface (airborne and spaceborne imaging spectroscopy). Recently, Jung et al. (2015) introduced a hyperspectral snapshot camera for proximal soil sensing.

The horizontal variability of soil surfaces is usually slow and gradual, but variability in the third dimension, depth, is much higher (Viscarra Rossel et al. 2015). Information on vertical variability is needed, among others, for interpretations of soil formation processes, characterizations of the soil horizons and the detection of small scale soil processes like bioturbation. The technique of laboratory imaging spectroscopy of soil cores using a hyperspectral line scanner was introduced by Buddenbaum & Steffens (2011) for spectroscopic analysis of undisturbed soil profiles with a very high spatial resolution. Applying this proximal sensing technique for the creation of elemental maps by using support vector regression and PLSR was presented by Buddenbaum & Steffens (2012b). Effects of spectral pre-treatments on elemental regressions using VNIR laboratory imaging spectroscopy were studied by Buddenbaum & Steffens (2012a). The approach was extended to include horizon classification and geostatistical characterization of a soil profile (Steffens & Buddenbaum 2013), and soil organic matter quality (Steffens et al. 2014). While these studies used only VNIR spectroscopy, SWIR cameras are now available with a comparable spatial resolution for laboratory use. Since many mineralogic absorption features are situated in the SWIR spectral region, an improved elemental mapping could be expected from adding SWIR information.

For the present study, soil cores were sampled from a Cambisol under Norway spruce and a Regosol under European beech stand close to Trier, Germany. Hyperspectral images of the cores were recorded using a VNIR camera and a SWIR camera. The content of C, N, Fe, Al, and Ca was analysed on reference samples with standard laboratory techniques. Spectra of the reference samples were used to establish regression models (PLS regression and MARS). These models were used to create maps of the elemental concentrations in the soil cores. Main research objectives were (1) to compare the regression techniques for elemental mapping of various elements, (2) to compare the predictive capacity of the VNIR and SWIR spectral range, and (3) to compare the two sampling sites in terms of elemental contents and distributions.

2 Material and Methods

2.1 *Study Site and Soil Sampling*

The sampling was carried out approximately 12 km northeast of Trier (Rhineland Palatinate, 49.84°N, 6.71°E). Two differing soil types were sampled. The first soil type was classified as an albic Cambisol under a Norway spruce monoculture, the second soil was a colluvic gleyic Regosol (WRB 2014) close to a creek under a European beech monoculture. Both soils derived from Triassic Sandstone (Buntsandstein). The study site is characterized by temperate, oceanic climate conditions with a mean annual temperature of 9.1 °C and a mean annual precipitation of 780 mm.

The soil profiles were sampled with custom-made stainless steel boxes. Two boxes with 100 × 100 × 300 mm³ size and two boxes with 100 × 100 × 500 mm³ were available. They were designed to sample undisturbed sections of soil profiles. After digging a hole and removing the litter layer, the steel boxes were gently hammered horizontally into the soil and subsequently excavated. In the lab, the soil cores were dried in the steel boxes at 35 °C for one week. Two profiles of different depths were sampled for each soil type, one of 30 cm and the other of 50 cm depth. The two profiles of albic Cambisol are subsequently indicated as Cambisol30 and Cambisol50, and the colluvic gleyic Regosol profiles as Regosol30 and Regosol50.

2.2 *Imaging Setup*

After smoothing the surface of the soil profile with a long knife, the images were recorded using a HySpex VNIR-1600 and a HySpex SWIR-320m-e hyperspectral camera (Norsk Elektro Optikk, Skedsmokorset, Norway) at the Department of Environmental Remote Sensing and Geoinformatics at the University of Trier (Buddenbaum & Hill 2015, Buddenbaum et al. 2015). The cameras were equipped with a 30 cm focal lens and set up in a laboratory frame with a translation stage under the camera. The translation stage moves the object in along-track direction, while the camera, a push-broom scanner, records image lines across track. The speed of the translation stage is adapted so that square pixels result.

For the VNIR images two tungsten halogen light sources illuminate the currently scanned line from about 35 cm distance and at an angle of about 45° in front of and behind the camera to minimize shadows on the soil surface. The VNIR-1600 camera records 1600 pixels across track with a field of view of 17°. The pixel instantaneous field of view is 0.18 mrad across track and 0.36 mrad along track. The area recorded from the 30 cm distance is 10 cm wide, so that the size of a single pixel amounts to about 63 µm. A 30 cm long soil profile consists of approximately 4800 image lines, a 50 cm profile of 8000 image lines. About 200 additional image lines containing a certified reflectance standard white reference panel of known reflectivity (Spectralon, Labspere Inc., North Sutton, NH, USA) were scanned with each sample, so radiance could be transformed to reflectance. 160 spectral bands were recorded in the spectral range of 414 nm to 1000 nm with a spectral sampling interval of 3.7 nm. The data was recorded in 12 bit radiometric resolution.

The laboratory frame can only hold one camera at a time, so the SWIR images were recorded after the VNIR datasets. Because the light source used for VNIR imaging only covers the spectral range up to 1700 nm, a stabilized tungsten halogen lamp (50 W) was used for illumination. The SWIR-320m-e camera records 256 spectral bands in the spectral range of 1000 nm to 2500 nm with a field of view of 13.5°. 320 pixels are acquired across track; a single pixel is about 250 µm wide. The 30 cm profiles consist of approximately 1200 lines, the 50 cm profiles of 2000 lines. The SWIR images were also recorded with a Spectralon white reference panel which covered about 50 lines.

2.3 *Image Pre-Processing*

Because the illumination was not perfectly uniform, the object reflectance ρ_{obj} was calculated for each image line (along track) separately following (1):

$$\rho_{obj} = \frac{L_{obj}}{L_{ref}} \cdot \rho_{ref} \quad (1)$$

where L_{obj} is the measured radiance from the object in camera units, L_{ref} is the measured radiance from the white reference and ρ_{ref} is the known reflectance of the white reference panel (Peddle et al. 2001).

Different pre-processing steps have been applied by several authors, e.g. Ben-Dor et al. (1997), Buddenbaum & Steffens (2012a), Udelhoven et al. (2003), and Viscarra Rossel & Webster (2011), but in combination with PLSR, these transformations were not able to increase regression accuracy significantly. To improve the signal-to-noise ratio, we applied spectral resampling, a bisection of the spatial resolution of the VNIR images, and continuum removal (CR). Spectral resampling implies an increase of the spectral sampling interval and the full width at half maximum from 3.7 nm to 7.3 nm in the VNIR range and from 7 nm to 15 nm in the SWIR range. With this transformation, neighbouring spectral bands were averaged, and the number of bands was reduced from 160 to 78 bands (VNIR) and from 256 to 100 bands (SWIR). The spatial resolution of the VNIR images was bisected by averaging 2×2 pixels to one resulting pixel. CR is a tool to amplify reflective features and especially to amplify absorption bands in a spectrum. This is done by fitting a convex hull to the spectrum and dividing the reflectance values for each wavelength by the reflectance level of the continuum line (convex hull) at the corresponding wavelength (Kokaly & Clark 1999). This pre-processing returns a CR value of 1 to all

parts of the spectrum that lie on the convex hull, i.e. wavelength regions that are not in an absorption band, and values between 0 and 1 to regions inside absorption bands. So CR accentuates the absorption bands in the spectra while minimizing brightness differences. The recorded images mostly have a high quality, but despite efforts to reduce noise, some noise is still present, especially in the SWIR range. The noise is most obvious in vertical stripes on the images.

To obtain spectra from 400 nm to 2500 nm for each pixel, an image-to-image geometric correction was applied. Ground control points (GCP) were identified in the images and used for warping the SWIR image to the VNIR image's geometry using a rubber sheeting (local triangulation) approach.

Homogeneous regions of interest (ROIs) of about 2 cm^2 area were regularly distributed over the soil profiles (18 ROIs on each of the 50 cm profiles and 12 ROIs on each of the 30 cm profiles) and mean spectra of these ROIs were extracted.

2.4 *Chemical Analysis*

The ROIs were visually identified in the soil core and samples of about 2 cm^2 and about 1 cm depth were taken for chemical laboratory analysis. After thoroughly sieving to < 2 mm and grinding, samples were oven-dried at 105 °C. Total organic carbon (TOC) and total nitrogen (TN) concentrations were determined in duplicate by dry combustion at 1100 °C by a EuroEA elemental analyzer (Hekatech GmbH, Wegberg, Germany) in carbonate-free samples. Total amounts of aluminum (Al), iron (Fe) and calcium (Ca) were extracted with 3 ml concentrated HNO_3 and 1 ml H_2O_2 (suprapur) in 0.1 g – 0.2 g dry mass using high pressure bombs (Berghof, Eningen, Germany) (Udelhoven et al. 2003). Element concentrations were measured with an atomic absorption spectrometer (Varian AA 240 FS and AA 240Z/GTA 120, Palo Alto, CA, U.S.A.).

2.5 *Elemental Mapping*

We compared two statistical methods for establishing regression models between elemental concentrations and reflective properties: Partial least-square regression (PLSR), and Multivariate adaptive regression splines (MARS). The regression analyses were carried out in MATLAB (Version R2012, Mathworks, Natick, MA, USA). All models were established on reflectance and chemical data from both soils and all horizons combined.

Partial least-square regression (PLSR) after Wold et al. (2001) is a widely used approach for quantitative analysis in chemometrics and hyperspectral remote sensing (Farifteh et al. 2007, Steffens & Buddenbaum 2013, Viscarra Rossel & Behrens 2010, Vohland & Emmerling 2011). PLSR is closely related to

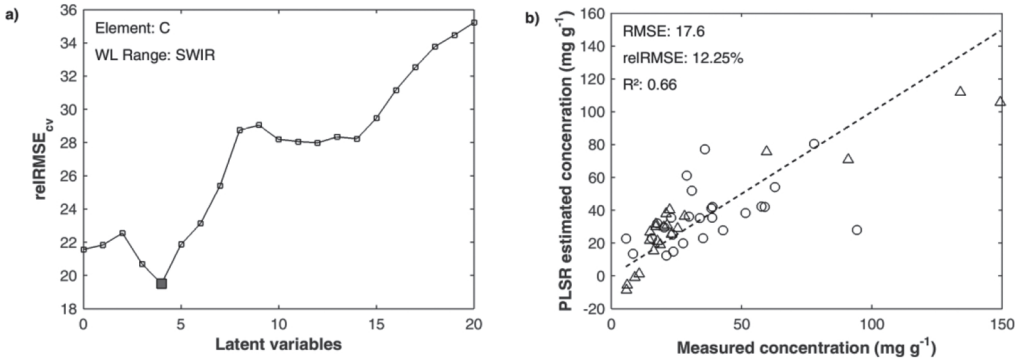

Fig. 1: PLS regression of C using the SWIR wavelength range: a) relative cross-validated RMSE as a function of the number of latent variables, best model at 4 latent variables is marked; b) measured versus C contents estimated using the model with 4 latent variables (Regosol: circles, Cambisol: triangles), and the 1:1 line.

principal components regression (PCR) and combines features from PCR and multiple regression (Marabel & Alvarez-Taboada 2013, Wold et al. 2001a). PLS regression projects the data (chemical concentrations and reflective properties with a high number of correlated variables) into a lower dimensional space, formed by a set of orthogonal latent variables, by a simultaneous decomposition of X (spectral matrix) and Y (chemical matrix) that maximizes the covariance between X and Y (Vohland & Emmerling 2011, Wold et al. 2001b). A large number of measured collinear spectral variables is reduced to a few non-correlated latent variables (Marabel & Alvarez-Taboada 2013), which also implements a reduction of the data volume and the calculation time. The method is well suited for the calibration of a small number of samples with experimental noise in both chemical and spectral data (Atzberger et al. 2010), even if the number of observations is smaller than the number of wavelengths (Ben-Dor et al. 2008).

To find the optimum number of latent variables, we calculated PLSR models with up to 20 latent variables on the ROI spectra for each analyzed element, separately for all VNIR-, SWIR-, and full range images. We applied a five-fold cross validation and a 100-fold Monte Carlo repetitions to each model to avoid overfitting (Schlerf et al. 2010) and calculated the cross-validated relative root-mean-square error (relRMSEcv) for each model.

Fig. 1a illustrates the relationship between number of latent variables and relRMSEcv. The model with lowest relRMSEcv was selected. With this optimal number of latent variables, a new PLSR is calculated and applied on the hyperspectral images to create maps of the distribution of the element in question. Resulting concentrations for C using the SWIR wavelength range and four latent variables compared to the laboratory measured concentrations are shown in Fig. 1b. No further calibration/validation scheme was applied, because plausible maps resulted from this strategy. Fig. 2 shows the regression coefficients (PLS weights) for each element and each wavelength range. The regression coefficients have been normalized for displaying them in the figure by subtracting their mean and dividing the result by their standard deviation (z-transformation). The plots show the important wavelength regions for estimating the elemental concentrations.

Multivariate adaptive regression splines (MARS) after Friedman (1991) is a non-parametric generalization of recursive partitioning

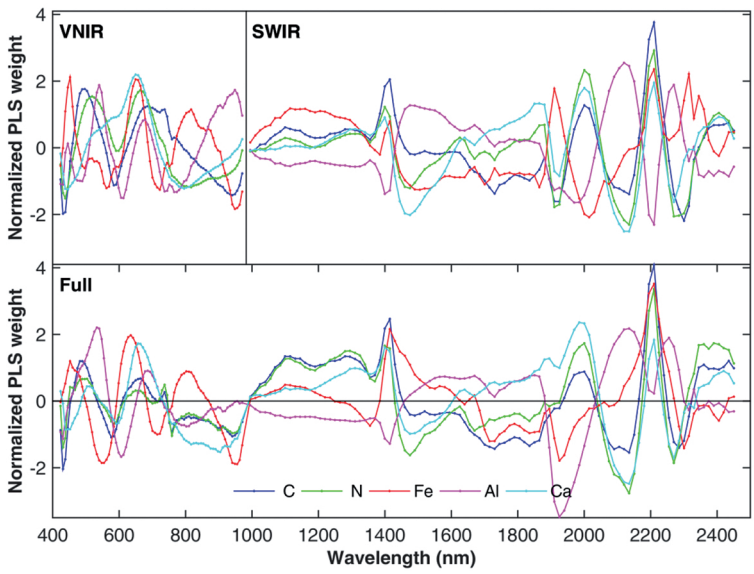

Fig. 2: Normalized weights of the input bands in the three PLS regressions (VNIR, SWIR, and full wavelength range).

regression approaches such as classification and regression trees (CART) (Viscarra Rossel & Behrens 2010). It makes no assumption about the underlying functional relationship between the dependent and independent variables. Nawar et al. (2015) found that MARS was better suited for the visible and near-infrared reflectance spectroscopy estimation of soil salinity than PLSR.

The MARS models were evaluated using a five-fold cross validation and 100 Monte Carlo repetitions. Elemental maps were then calculated by applying the models on a pixel-by-pixel basis on the hyperspectral images.

Even though the profiles were illuminated from two directions, the formation of shadow because of strong surface roughness was unavoidable. Parts of the profiles with high carbon and nitrogen or iron-concentrations are dark coloured. The spectral signatures of these parts are similar to the shadow signatures, which results in false values. To correct this, shadows had to be determined and the profiles shadow masked. Shadows were detected using a principal component analysis followed by an unsupervised classification. One of the resulting classes corresponded well with shadowed areas in a visual inspection. After building a shadow mask for each profile, this mask was applied on the respective image (Steffens & Buddenbaum 2013).

3 Results and Discussion

3.1 *Elemental Concentrations*

The high variance of carbon and nitrogen content in both soils are shown in Tabs. 1 and 2. Typically, in both soils a vertical element gradient was clearly developed with high organic matter content in the topsoil and decreasing amounts with increasing depth. The thickness of the humus-rich A-horizon ranged from 6 cm to 10 cm depending on the respective soil profile. Mean concentrations of TOC in the topsoil reached more than 200 mg g^{-1}, whereas in the subsoil it was about 20 mg g^{-1} – 30 mg g^{-1}. Nitrogen showed the same trend, with amounts in a range from 0.2 mg g^{-1} – 16 mg g^{-1}. Maximum C contents of 291 mg g^{-1} (Cambisol) or 339 mg g^{-1} (Regosol) might be attributed to residues of the litter layers, which have not been involved in the soil sampling schedule. Both soils derived from siliceous bedrocks (Sandstones) and thus, as expected, soil pH in these soils varied between 4.5 and 5.0, which is equivalent to the silicate buffer capacity of soil. As a consequence, soils were carbonate-free and thus, amounts of total carbon in soil were equivalent to total organic carbon.

Amounts of Fe, Al, and Ca in both soils showed a different element distribution in the soil profile compared to carbon and nitrogen. Although there was a remarkable variability in the amounts of Fe and Al, the differences in both elements between the top soils and the sub-soils of both investigated soil profiles remained small. The differences in the element distribution of Fe and Al between both soils were also quite small and in a typical range of those soils. Similarly, Ca was concentrated in the top soil and amounts of Ca in the subsoil were in both soils roughly at the detection limit. This result can also be attributed to the parent material and forestal land-use of both soils.

Tab. 1: Descriptive statistics of the Regosol including minimum (Min), maximum (Max), mean of concentrations of all five elements. Negative values result from detection limits in the analysis and were treated as zero in further analyses.

Colluvic Gleyic Regosol					
	C (mg g^{-1})	N (mg g^{-1})	Fe (mg g^{-1})	Al (mg g^{-1})	Ca (mg g^{-1})
Min	5.7	0.2	0.44	3.26	-0.42
Max	338.8	16.1	4.66	17.06	1.77
Mean Topsoil	270.8	13.4	3.42	3.63	1.26
Mean Subsoil	36.5	1.7	1.36	9.35	-0.10
Mean full profile	71.2	3.5	1.66	8.50	0.10

Tab. 2: Descriptive statistics of the albic Cambisol containing minimum (Min), maximum (Max), mean of concentrations of all five elements in their specific units. Negative value results from detection limits in the analysis and was treated as zero in further analyses.

	Albic Cambisol				
	C (mg g^{-1})	N (mg g^{-1})	Fe (mg g^{-1})	Al (mg g^{-1})	Ca (mg g^{-1})
Min	5.9	0.2	1.70	4.11	-0.16
Max	290.7	10.4	5.54	15.60	2.83
Mean Topsoil	199.7	7.3	3.05	5.69	1.57
Mean Subsoil	24.5	0.8	3.05	8.09	-0.02
Mean full profile	50.5	1.8	3.05	7.73	0.22

Tab. 3: Intercorrelations of the elemental concentrations.

	C	N	Fe	Al	Ca
C	1				
N	0.979	1			
Fe	0.286	0.259	1		
Al	-0.318	-0.324	-0.027	1	
Ca	0.897	0.831	0.255	-0.329	1

Tab. 4: Statistical comparison of the PLSR models. For each element and wavelength range statistically best result (relRMSE and R^2) and corresponding number of latent variables (LV) is listed. Data for the two soils are combined.

	VNIR			SWIR			Full		
	relRMSE / %	R^2	#LV	relRMSE / %	R^2	#LV	relRMSE / %	R^2	#LV
C	15.32	0.468	4	12.25	0.660	4	**10.13**	**0.767**	**7**
N	12.54	0.601	3	9.44	0.774	4	**8.16**	**0.831**	**7**
Fe	9.78	0.818	7	17.55	0.415	4	**9.58**	**0.826**	**7**
Al	21.71	0.340	5	21.02	0.381	4	**19.42**	**0.472**	**5**
Ca	9.68	0.767	3	7.82	0.848	4	**6.34**	**0.900**	**6**

Tab. 5: Statistical comparison of the MARS models. Best results are displayed in bold. Data for the two soils are combined.

	VNIR		SWIR		Full	
	relRMSE	R^2	relRMSE	R^2	relRMSE	R^2
C	25.27	0.250	30.86	0.215	**24.62**	**0.300**
N	22.08	0.209	24.42	0.285	**19.77**	**0.353**
Fe	**18.84**	**0.451**	30.91	0.130	22.45	0.339
Al	**27.91**	**0.186**	33.38	0.101	32.59	0.126
Ca	**12.50**	**0.682**	16.04	0.629	14.55	0.632

Intercorrelations between the elemental concentrations are listed in Tab. 3. C and N are very highly correlated with each other and highly correlated with Ca. Fe and Al show no correlation with each other and low correlations with the other elements.

3.2 *Regression Models of Elemental Concentrations*

For each element, multiple concentrations maps (derived from different wavelengths ranges: VNIR, SWIR, and full range) were calculated combining data from the two soils. relRMSE and R^2 of the statistically best results are shown for each element and each wavelength range in Tabs. 4 and 5 for PLSR and MARS, respectively.

Using PLSR, most elements are estimated best with the full wavelength range. Surprisingly, C estimations using SWIR data are better than VNIR-based estimations, although it is well known that a high organic carbon amount colours the soil dark in the visible spectral region (Stoner & Baumgardner 1981).

Tab. 5 gives an overview of the statistical results using MARS. In the visual comparison, almost all MARS maps were inferior to the PLSR maps, and R^2 and relRMSE values of the MARS models are lower than the PLSR values, which is in contrast to the results of Nawar et al. (2014). Best statistical values for the organic matter (C and N) are in the full wavelength range. Best models for Fe, Al, and Ca are in the VNIR wavelength range, which is plausible for iron because of the broad absorption bands between 0.6 µm and 1.5 µm (Mulders 1987). Fig. 3 shows scatter plots of MARS estimations of C for the three wavelength regions. The scatter plot in the VNIR wavelength range shows a narrow distribution of most samples on the 1:1 line for the lower values, but some strong outliers in the range above 50 mg g^{-1} (Fig. 3a). The distribution in the SWIR wavelength range is generally similar, with one outlier even far in the negative range (Fig. 3b). R^2 in the SWIR is lowest and RMSE is highest. In the full wavelength range the scatter is still high, but outliers are less extreme and thus the highest R^2 and lowest RMSE values are achieved (Fig. 3c). The high amount of image noise in the resulting maps and the fact that in most cases the full wavelength range does not lead to the highest accuracies hint to some sensitivity to noise and overfitting in MARS.

Selected elemental maps showing the strengths and weaknesses of the statistical results are discussed. Fig. 4 displays PLSR-derived maps of the five elements for the profile Cambisol50. Each map covers a profile area of 10 cm width and 50 cm depth. All maps reflect the spatial distribution well and have plausible ranges of values. C mainly accumulates in the top-horizon, but also in the subsoil, isolated organic residues are recognizable, e.g. caused by roots. Due to the very high correlation between C and N contents, the N map has similar distributions; organic residues in the subsoil region are even better recognizable in the nitrogen map than in the C map. The Fe content is relatively homogenous throughout the profile because of the iron-rich parent material. Al shows a pattern similar to Fe, but the maximum is in a lower region of the profile.

The Ca profile in Fig. 4 has to be discussed carefully, because concentrations in the subsoils (of both soils) were sometimes under the detection limit. There are some patches of Ca concentrations which might have remained from previous liming events.

Fig. 5 shows a comparison of C in the Cambisol30 profiles created using the three wavelength ranges and PLS regression. In the VNIR profile, accumulations of C are visible in the humus-rich top soil and in organic residues (roots) in the subsoil regions. The SWIR profile accentuates regions of high C content more strongly. The full range data leads to the most contrast-rich map of C but also shows the most image noise.

Some maps created with MARS can be seen in Fig. 6. While C, N, and Al are mapped in acceptable quality, the maps of Fe and Ca are quite noisy. According to the reference measurements, C and N concentrations are highest in the topsoil, but MARS is unable to capture that.

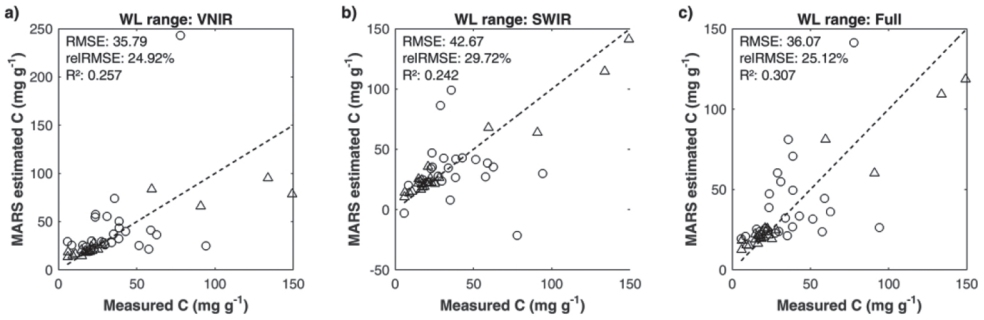

Fig. 3: Measured against MARS estimated C concentrations (with 1:1 lines) using different wavelength ranges (Regosol: circles, Cambisol: triangles).

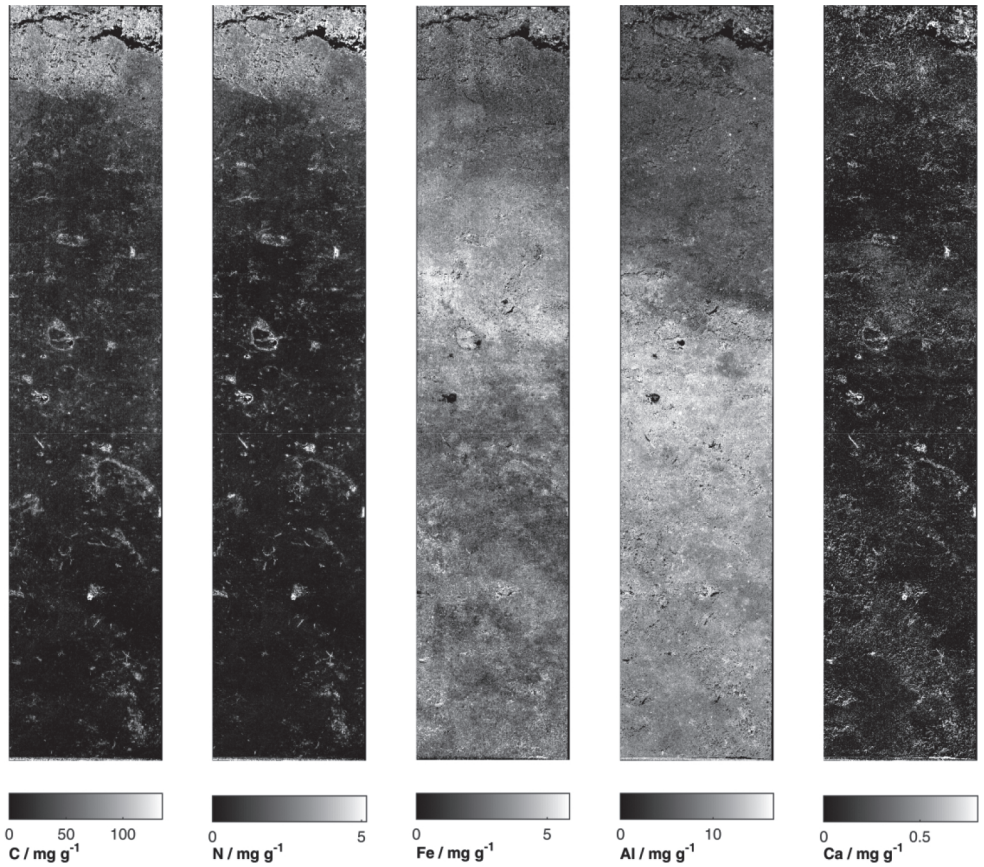

Fig. 4: Maps of the 5 elements in the 50 cm long Cambisol profile according to PLS regression using the full wavelength range. The grey levels are stretched linearly from 0 (black) to the 98th percentile of values present in each map (white).

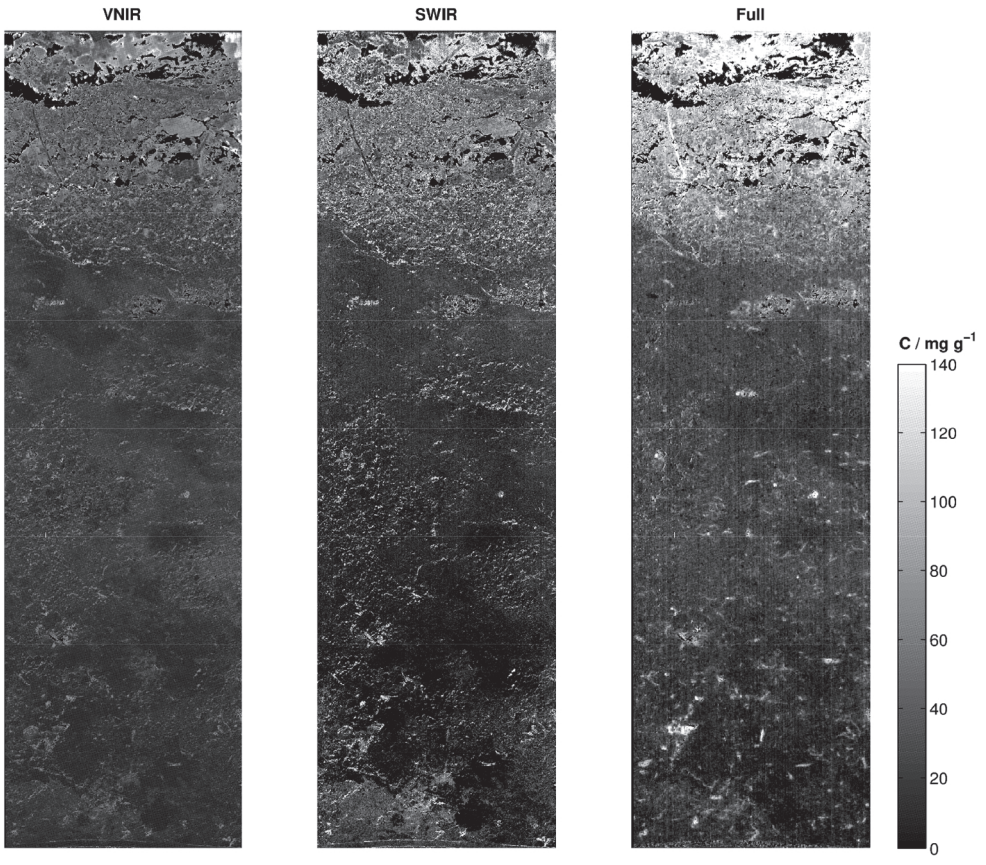

Fig. 5: Comparison of PLSR C maps of the Cambisol30 profile created with three different wavelength ranges. The grey levels are stretched linearly from 0 (black) to the 98th percentile of value of the full range map (white).

4 Conclusions

In this study, elemental concentrations in soil profiles were mapped using laboratory imaging spectroscopy. We compared three spectral ranges, i.e. VNIR, SWIR, and full range images, and two regression methods, i.e. MARS and PLSR.

PLSR was better suited for elemental mapping, both in terms of statistical measures and in visual quality of the resulting maps. This study confirms PLSR as a powerful regression tool that makes use of all input bands and serves well in identifying important spectral bands representing specific elemental concentrations in natural soil profiles. PLSR is less affected by image noise, while the MARS maps emphasize the noise that is present in the image data.

While previous studies used exclusively the VNIR camera, the additional information retrieved using a SWIR camera was tested in this study. The elemental maps using only the HySpex SWIR-320m-e module were not always reasonable, but regressions including VNIR and SWIR wavelengths in combination lead to improved statistical results.

The resulting maps show elemental distribution in a very high spatial resolution and can be used for further analyses of the soil cores and their horizons. Consequently, laboratory imaging spectroscopy of soil profiles in the

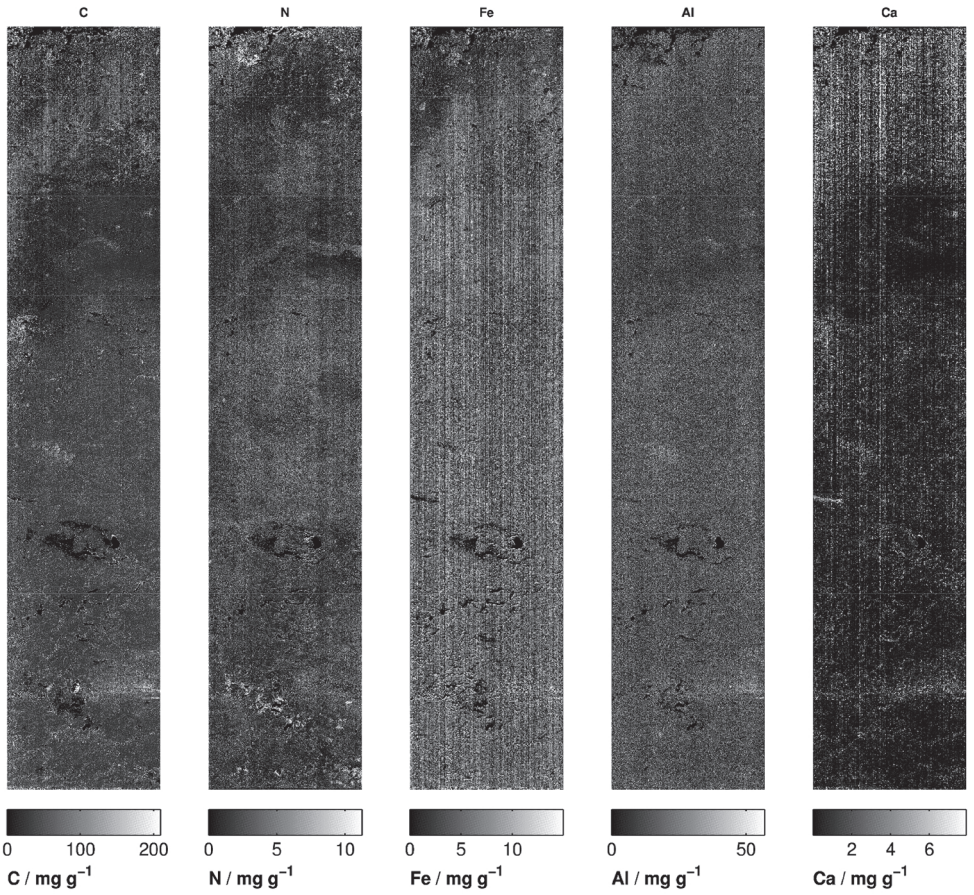

Fig. 6: Maps of the 5 elements in the 50 cm long Regosol profile according to MARS regression. The grey levels are stretched linearly from 0 (black) to the 98th percentile of values present in each map (white).

VNIR/SWIR range has proved to be a promising and reliable novel technique for various soil scientific topics.

Acknowledgements

We thank Joachim Hill from the Department of Environmental Remote Sensing and Geoinformatics at the University of Trier for providing the imaging spectrometer, and Peter Schad of the Chair of Soil Science at TU München for help with the WRB classification.

References

Atzberger, C., Guérif, M., Baret, F. & Werner, W., 2010: Comparative analysis of three chemometric techniques for the spectroradiometric assessment of canopy chlorophyll content in winter wheat. – Computers and Electronics in Agriculture **73** (2): 165–173.

Ben-Dor, E., Inbar, Y. & Chen, Y., 1997: The reflectance spectra of organic matter in the visible near-infrared and short wave infrared region (400 nm – 2500 nm) during a controlled decomposition process. – Remote Sensing of Environment **61** (1): 1–15.

Ben-Dor, E., Heller, D. & Chudnovsky, A., 2008: A Novel Method of Classifying Soil Profiles in the Field using Optical Means. – Soil Science Society of America Journal **72** (4): 1113–1123.

Ben-Dor, E., Chabrillat, S., Demattê, J.A.M., Taylor, G.R., Hill, J., Whiting, M.L. & Sommer, S., 2009: Using Imaging Spectroscopy to study soil properties. – Remote Sensing of Environment **113** (Supplement 1): S38–S55.

Buddenbaum, H. & Steffens, M., 2011: Laboratory imaging spectroscopy of soil profiles. – Journal of Spectral Imaging **2** (a2): 1–5.

Buddenbaum, H. & Steffens, M., 2012a: The Effects of Spectral Pretreatments on Chemometric Analyses of Soil Profiles Using Laboratory Imaging Spectroscopy. – Applied and Environmental Soil Science **2012:** 12.

Buddenbaum, H. & Steffens, M., 2012b: Mapping the distribution of chemical properties in soil profiles using laboratory imaging spectroscopy, SVM and PLS regression. – EARSeL eProceedings **11** (1): 25–32.

Buddenbaum, H. & Hill, J., 2015: PROSPECT Inversions of Leaf Laboratory Imaging Spectroscopy – a Comparison of Spectral Range and Inversion Technique Influences. – PFG – Photogrammetrie, Fernerkundung, Geoinformation **2015** (3): 231–240.

Buddenbaum, H., Stern, O., Paschmionka, B., Hass, E., Gattung, T., Stoffels, J., Hill, J. & Werner, W., 2015: Using VNIR and SWIR Field Imaging Spectroscopy for Drought Stress Monitoring of Beech Seedlings. – International Journal of Remote Sensing **36** (18): 4590–4605.

Farifteh, J., Van der Meer, F.D., Atzberger, C. & Carranza, E.J.M., 2007: Quantitative analysis of salt-affected soil reflectance spectra: A comparison of two adaptive methods (PLSR and ANN). – Remote Sensing of Environment **110:** 59–78.

Farifteh, J., van der Meer, F., van der Meijde, M. & Atzberger, C., 2008: Spectral characteristics of salt-affected soils: A laboratory experiment. – Geoderma **145** (3–4): 196–206.

Friedman, J. H., 1991: Multivariate Adaptive Regression Splines. – The Annals of Statistics **19** (1): 1–67.

Hartemink, A.E. & Minasny, B., 2014: Towards digital soil morphometrics. – Geoderma **230–231:** 305–317.

Heinze, S., Vohland, M., Joergensen, R. G. & Ludwig, B., 2013: Usefulness of near-infrared spectroscopy for the prediction of chemical and biological soil properties in different long-term experiments. – Journal of Plant Nutrition and Soil Science **176** (4): 520–528.

Jung, A., Vohland, M. & Thiele-Bruhn, S., 2015: Use of A Portable Camera for Proximal Soil Sensing with Hyperspectral Image Data. – Remote Sensing **7** (9): 11434.

Kokaly, R.F. & Clark, R.N., 1999: Spectroscopic Determination of Leaf Biochemistry Using Band-Depth Analysis of Absorption Features and Stepwise Multiple Linear Regression. – Remote Sensing of Environment **67** (3): 267–287.

Marabel, M. & Alvarez-Taboada, F., 2013: Spectroscopic Determination of Aboveground Biomass in Grasslands Using Spectral Transformations, Support Vector Machine and Partial Least Squares Regression. – Sensors **13** (8): 10027–10051.

Mulders, M.A., 1987: Remote Sensing in Soil Science. – Elsevier Science Publishers B.V., Amsterdam, The Netherlands, ISBN: 978-0-444-42783-0.

Nawar, S., Buddenbaum, H., Hill, J. & Kozak, J., 2014: Modelling and Mapping of Soil Salinity with Reflectance Spectroscopy and Landsat Data Using Two Quantitative Methods (PLSR and MARS). – Remote Sensing **6** (11): 10813–10834.

Nawar, S., Buddenbaum, H. & Hill, J., 2015: Estimation of soil salinity using three quantitative methods based on visible and near-infrared reflectance spectroscopy: a case study from Egypt. – Arabian Journal of Geosciences **8** (7): 5127–5140.

Peddle, D.R., White, H.P., Soffer, R.J., Miller, J.R. & LeDrew, E.F., 2001: Reflectance processing of remote sensing spectroradiometer data. – Computers & Geosciences **27** (2): 203–213.

Schlerf, M., Atzberger, C., Hill, J., Buddenbaum, H., Werner, W. & Schüler, G., 2010: Retrieval of chlorophyll and nitrogen in Norway spruce (Picea abies L. Karst.) using imaging spectroscopy. – International Journal of Applied Earth Observation and Geoinformation **12** (1): 17–26.

Steffens, M. & Buddenbaum, H., 2013: Laboratory imaging spectroscopy of a stagnic luvisol profile – High resolution soil characterisation, classification and mapping of elemental concentrations. – Geoderma **195–196:** 122–132.

Steffens, M., Kohlpaintner, M. & Buddenbaum, H., 2014: Fine spatial resolution mapping of soil organic matter quality in a Histosol profile. – European Journal of Soil Science **65** (6): 827–839.

Stenberg, B., 2010: Effects of soil sample pretreatments and standardised rewetting as interacted with sand classes on Vis-NIR predictions of clay and soil organic carbon. – Geoderma **158** (1–2): 15–22.

Stoner, E.R. & Baumgardner, M.F., 1981: Characteristic Variations in Reflectance of Surface Soils. – Soil Science Society of America Journal **45:** 1161–1165.

Udelhoven, T., Emmerling, C. & Jarmer, T., 2003: Quantitative analysis of soil chemical properties with diffuse reflectance spectrometry and partial least-square regression: A feasibility study. – Plant and Soil **251:** 319–329.

Viscarra Rossel, R.A., Walvoort, D.J.J., McBratney, A.B., Janik, L.J. & Skjemstad, J.O., 2006: Visible, near infrared, mid infrared or combined diffuse reflectance spectroscopy for simultaneous assessment of various soil properties. – Geoderma **131** (1–2): 59–75.

Viscarra Rossel, R.A., Cattle, S.R., Ortega, A. & Fouad, Y., 2009: In situ measurements of soil colour, mineral composition and clay content by vis-NIR spectroscopy. – Geoderma **150** (3–4): 253–266.

Viscarra Rossel, R.A. & Behrens, T., 2010: Using data mining to model and interpret soil diffuse reflectance spectra. – Geoderma **158** (1–2): 46–54.

Viscarra Rossel, R.A. & Webster, R., 2011: Discrimination of Australian soil horizons and classes from their visible-near infrared spectra. – European Journal of Soil Science **62** (4): 637–647.

Viscarra Rossel, R.A., Chen, C., Grundy, M.J., Searle, R., Clifford, D. & Campbell, P.H., 2015: The Australian three-dimensional soil grid: Australia's contribution to the GlobalSoilMap project. – Soil Research, CSIRO Publishing.

Vohland, M., Bossung, C. & Fründ, H.-C., 2009: A spectroscopic approach to assess trace-heavy metal contents in contaminated floodplain soils via spectrally active soil components. – Journal of Plant Nutrition and Soil Science **172** (2): 201–209.

Vohland, M. & Emmerling, C., 2011: Determination of total soil organic C and hot water-extractable C from VIS-NIR soil reflectance with partial least squares regression and spectral feature selection techniques. – European Journal of Soil Science **62** (4): 598–606.

Wold, S., Sjöström, M. & Eriksson, L., 2001a: PLS-regression: a basic tool of chemometrics. – Chemometrics and Intelligent Laboratory Systems **58** (2): 109–130.

Wold, S., Trygg, J., Berglund, A. & Antti, H., 2001b: Some recent developments in PLS modeling. – Chemometrics and Intelligent Laboratory Systems **58** (2): 131–150.

WRB, I.W.G., 2014: World Reference Base for Soil Resources 2014. – FAO International soil classification system for naming soils and creating legends for soil maps 106, Rome, Italy.

Addresses of the Authors:

Simon Schreiner & Dr. Henning Buddenbaum, University of Trier, Environmental Remote Sensing & Geoinformatics, D-54286 Trier, Germany, Tel.: +49-651-201-4729, e-mail: {s6sischr}{buddenbaum}@uni-trier.de

Prof. Dr. Christoph Emmerling, University of Trier, Soil Science, D-54286 Trier, Germany, e-mail: emmerling@uni-trier.de

Dr. Markus Steffens, Lehrstuhl für Bodenkunde, Department für Ökologie und Ökosystemmanagement, Wissenschaftszentrum Weihenstephan für Ernährung, Landnutzung und Umwelt, Technische Universität München, D-85350 Freising-Weihenstephan, Germany, e-mail: steffens@wzw.tum.de

Manuskript eingereicht: September 2015
Angenommen: Oktober 2015

PFG 2015 / 6, 0437–0448
Stuttgart, December 2015

Article

The Impact of different Leaf Surface Tissues on active 3D Laser Triangulation Measurements

Jan Dupuis, Bonn, Stefan Paulus, Aachen, Anne-Katrin Mahlein, Heiner Kuhlmann & Thomas Eichert, Bonn

Keywords: 3D laser scanning, laser intensity, tissue penetration, optical properties of leaf surfaces, plant disease detection

Summary: Laser scanning devices used for plant phenotyping have shown their ability to penetrate the plant surface. This results in an interaction with the leaf tissue and in absorption of the emitted laser. The use of the intensity of reflection, measured from the backscattered laser ray, enables a more profound analysis of the geometric accuracy as well as an inspection of the plant's physiological condition. We show the comparison of two triangulation-based 3D laser scanners with different wavelengths, 658 nm (red) and 405 nm (blue), providing the intensity as additional information. By analysing the interaction of both laser sensors with separated leaf tissue contents it is possible to locate the origin of the measured signal and to evaluate the geometric accuracy of the point cloud. Furthermore, differences in the physiology of the plant as well as surface altering plant diseases like powdery mildew can be identified using the intensity of reflection. The use of the combination of a blue and a red laser scanner for high precision 3D imaging of the plant surface is shown, as well as its applicability for the analysis of plant tissue composition, the stage of leaf senescence and for a detection of plant diseases is demonstrated. Finally, the intensity of the red laser showed a high interpretability regarding the tissue composition while the blue laser provided a high geometric accuracy.

Zusammenfassung: *Einfluss von unterschiedlichen Blattschichten auf 3D Laser-Triangulation.* Bei der Phänotypisierung von Pflanzen mittels Laserscannern hat sich gezeigt, dass der ausgesandte Laser in die Pflanzenstruktur eindringt und dort von den photoaktiven Bestandteilen teilweise absorbiert wird. Die Nutzung zusätzlicher Messinformationen wie der Intensität des Messsignals ermöglicht es, eine detailliertere Aussage über den Ursprung der Reflexion und somit auch über die geometrische Genauigkeit zu treffen. Zusätzlich können Aussagen über den physiologischen Zustand der Pflanzen abgeleitet werden. Die Studie nutzt zwei 2D-Lasertriangulationssensoren mit unterschiedlichen Wellenlängen, 658 nm (rot) und 405 nm (blau), mit deren Hilfe die Interaktion verschiedener Laserfarben mit separierten Blattbestandteilen untersucht wird. Durch Einbeziehen der Intensität ist es möglich, den Ursprung der Reflexion zu lokalisieren und systematische Abweichungen der resultierenden Punktwolke aufzudecken. Darüber hinaus unterstützt die Intensität die Analyse des physiologischen Zustands der Pflanze und ermöglicht die Detektion oberflächenverändernder Pflanzenkrankheiten wie dem Echten Mehltau. Letztlich kann gezeigt werden, dass die Kombination zweier Laserfarben sowohl die Interpretierbarkeit als auch die geometrische Genauigkeit der gemessenen Punktwolke verbessert.

1 Introduction

Highly accurate 3D plant measurements have become an important tool for plant phenotyping (Omasa et al. 2007). 3D measurements are performed at different scales from airplanes, with fixed-positioned terrestrial laser scanners and with experimental close-up laser setups. The scales of the analysed objects comprise the canopy structure (Næsset & Bjerknes 2001), single trees (Pfeifer et al. 2004) and single plants on organ level (Paulus et al. 2013, Paulus et al. 2014b, Wahabzada et al. 2015), respectively.

www.schweizerbart.de
DOI: 10.1127/pfg/2015/0280
1432-8364/15/0280 $ 3.00

In particular, high throughput phenotyping focuses on the monitoring of plant and organ development (Honsdorf et al. 2014) as well as on the derivation of phenotypic parameters from processed point clouds (Paproki et al. 2012, Bellasio et al. 2012). Industrial measuring systems using active laser triangulation were commonly applied for plant measurements, providing a spatial resolution and geometrical accuracy of sub-millimetres (Paulus et al. 2014a, Wagner et al. 2010). This is essential for the tracking of growth and smallest geometrical changes due to environmental conditions like nutrient availability or abiotic and biotic stress (Paulus et al. 2014d).

Evaluating the accuracy of 3D plant measurements is extremely challenging, because no highly accurate reference systems are available. For industrial purposes high accurate reference artifacts can be provided that enable the analysis of the sensor quality (Dupuis & Kuhlmann 2014). Furthermore, recent research has shown that the plant-sensor interaction is not negligible (Paulus et al. 2014c). Sensor properties like laser wavelength and exposure time have a significant impact on the resulting 3D point cloud. The received signal, backscattered from different layers of the plant structure, is partially absorbed by chlorophyll and, in the worst case, it results in a sensor signal that is not evaluable.

The physical effect of the penetration of laser light into the surface structure of different materials as well as the depth of the penetration is well known in dermatology (Barolet 2008) and photodynamic therapy (Mustafa & Jaafar 2012). In this context, it is of high importance to treat the human skin in defined tissue depths. For wavelengths between 300 nm and 900 nm, experiments and simulations pointed out that longer wavelengths lead to larger physical penetration (Barolet 2008). Furthermore, spectral analysis has shown that the absorption by plant tissue strongly depends on the used wavelength (Fiorani et al. 2012). As established commercial 3D measuring devices mainly use a red laser light that lies in the absorption maximum of chlorophyll, the use of a different wavelength should improve the scanning result and the interpretability (Strothmann et al. 2014). The work of Wei et al. (2012) showed the application of up to four laser wavelengths in a multi-wavelength canopy LiDAR for the detection and classification of biochemical concentrations, e.g. withered *vs.* healthy leaves on canopy level.

Apart from these physical effects, based on a metrological viewpoint, there is the question how the surface penetration and the spectral properties of plants affect the results of commercial laser scanning devices. For materials such as marble, it has been shown that the distance measurement is affected systematically, which results in a reduced measurement accuracy (Dupuis & Kuhlmann 2014).

Therefore, we show a combined 3D laser scanning approach using two commercial triangulation-based laser scanners with different wavelengths (405 nm and 658 nm), providing the intensity of the backscattered laser ray as additional information. In contrast to Paulus et al. (2014c), where the analysis was based on the point density using several scans with different sensor settings, the intensity enables the direct and repeatable analysis of the reflectance depth of the signal and a better understanding of the interaction of the laser with the leaf surface structures. Based on the intensity values we are able to locate the origin of the received signal and to analyse the accuracy of the 3D point cloud. Furthermore, we show that an intensity based analysis provides more profound insights into the stage of leaf senescence of the plants combined with the geometrical surface information in 3D.

2 Measuring Setup

Laser scanning experiments were performed using a measuring system comprising a 2D laser triangulation sensor (LTS), working according to the light-section method (Donges & Noll 1993), and a moving table. A linear guidance system, combined with a stepper motor (isel Germany AG, Eichenzell, Germany) that actuates the moving table, supplements the 2D laser sensor with the third dimension (Fig. 1A, B), i.e. the scanner is mounted in a fixed position above the moving table and the measured object is moved through its vertical laser plane. The table was moved stepwise, i.e. the measurement was performed when the object under test was static. According to investigations

using special reference artifacts, the precision of the measuring system is σ = 20 µm (standard deviation) (Dupuis & Kuhlmann 2014).

The measuring system was originally equipped with a commercial laser sensor (scanCONTROL 2700-100, MICRO-EPSILON MESSTECHNIK GmbH & Co. KG, Ortenburg, Germany) providing a wavelength of 658 nm (red). Latest developments in sensor technology allow the use of an alternative wavelength of 405 nm (blue) in a commercial high-precision laser sensor. Thus, we decided to extend the measuring system with an extra laser line scanner (gapCONTROL 2911-100 BL). To overcome interferences between the two sensors the measuring system was only equipped with one sensor during the measurement and the sensors were exchanged afterwards.

The two-dimensional field of view of both sensors is limited to a window of 100 mm × 100 mm at a spatial resolution of 5µm in distance and ~150 µm in the lateral position. The theoretical accuracy for the distance measurement provided by the manufacturer is 15 µm for the red and 12 µm for the blue laser sensor.

In addition to the access to Euclidean coordinates and the geometrical shape of plants' surface, the data analysis is based on the intensity that is provided by both laser scanners. This additional information is determined as the maximum amount of reflected laser light collected in each column of the CCD-array. The intensity is given as a relative value in %, which describes the amount of photons in one pixel element compared to the maximum possible amount of photons. Thus, using a fixed exposure time, these intensity values can be interpreted as reflectance values of the measured surface for every 3D point.

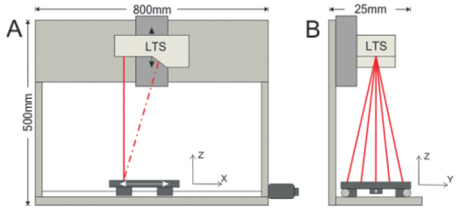

Fig. 1: The technical setup of the measuring system in front (A) and side view (B), LTS = laser triangulation sensor (Dupuis & Kuhlmann 2014).

3 Impact of different Leaf Tissues

The main objective of this study is to present the impact of the characteristics of leaf or plant surfaces on measurements performed by an active 3D laser triangulation sensor. The experiments focus on the interaction of the laser sensor with the leaf surface and on the way in which this will affect the measurement accuracy. They were inspired by a previous publication (Paulus et al. 2014c) where the data interpretation was based on the point density measured at different exposure times ranging from the minimum to the maximum limit of the laser sensor. In the present study, an intensity-based data analysis was utilized, thus it was possible to analyse single measurements using one fixed exposure time. However, measurements were performed up to 10 times to prove their repeatability. As all repetitions follow the same behaviour, representative results for one measurement were shown. The exposure time was manually set to a level with a minimum amount of over- and underexposure of the CCD-array to achieve highest geometric measurement accuracy and to minimize systematic uncertainties (Dupuis & Kuhlmann 2014). However, as we used natural objects with various reflective properties, over- or underexposure cannot be excluded entirely.

3.1 *Measurability of Epidermis*

In theory, the epidermis, a single layer of cells that forms the boundary between the plant and the environment, is lacking chlorophyll and, thus, is almost transparent compared to the mesophyll cells. To visualize the effect of the physical penetration depth on the measured point cloud, different numbers of epidermal stripes extracted from leek leaves (*Allium porrum* L.) were scanned with both lasers. The physical penetration of the laser beam into the surface structure causes a systematic deviation of the distance measurement and, therefore, the measured surface does not represent the real surface. This deviation, afterwards called measured penetration depth, may differ from the physical penetration depth and is described for different types of laser sensors and

different surfaces, e.g. terrestrial laser scanners (Gordon 2008) and laser triangulation sensors (Dupuis & Kuhlmann 2014).

The epidermal strips were separated carefully using a razor blade and were attached subsequently in a flat way on a microscope slide made of glass (Fig. 2A–C). As we were interested in the measured depth of penetration, three different test objects were created having an increasing number of epidermal strips of one to three layers.

From the measured point clouds, regions representing the epidermal layer were selected manually and a best-fit plane was estimated using a least-square approach (Mikhail & Ackermann 1976). The underlying microscope slides were prepared with black stripes that represent an impenetrable pattern on the glass surface. Based on this setup, measurements without the epidermal stripes (Fig. 2D) would result in a point distribution as illustrated in Fig. 2E. In this case, the estimated plane would lie approximately in the middle of the microscope slide and the residuals would represent the pattern of the black stripes.

Scanning the epidermal stripes attached on top of the slides (Fig. 2F) could theoretically create two different results. The first one, shown in Fig. 2G, will be achieved, if the epidermis is impenetrable. In this case the point cloud represents the real geometric surface, as it is expected for blue laser sensor. The second possible outcome, shown in Fig. 2H, will be similar to the point cloud in Fig. 2E, but attenuated, and will be achieved if the epidermis is transparent or semi-transparent. Based on these considerations one can assume that if the pattern of the black stripes is visible in the residuals of the best-fit plane, the laser scanner will be able to penetrate the epidermis and to measure the underlying surface tissues.

Fig. 3 shows the point clouds of both laser colours for the different numbers of epidermal layers. The colour information represents the residuals of the best-fit plane. In Fig. 3A, the stripe pattern is clearly visible – comparable to the theoretical pattern in Fig. 2E – with a maximum positive deviation from the estimated plane of ~0.5 mm (blue stripes). The regions with red colour constitute points with a maximum negative deviation from the plane, i.e. the distance measured by the sensor is larger, which in turn is attributable to a physical penetration of the laser light through the epidermis and the microscope slide. Fig. 3A illustrates the measurement of one epidermal layer with the red laser sensor. Accordingly, one epidermal layer measured with the red laser scanner leads to a transmission of the laser light. A similar but weaker effect is visible in case of two or three epidermal layers (Fig. 3B, C).

The measurements performed with the blue laser sensor show a different behaviour (Fig. 3D–F). The black strips are only visible in case of one epidermal layer with a deviation of about 0.1 mm. Even parts of the regions between these strips provide a very small deviation value. These smaller deviations can be related to a much smaller physical and measured penetration depth. Furthermore, the results for two and three epidermal layers do not show

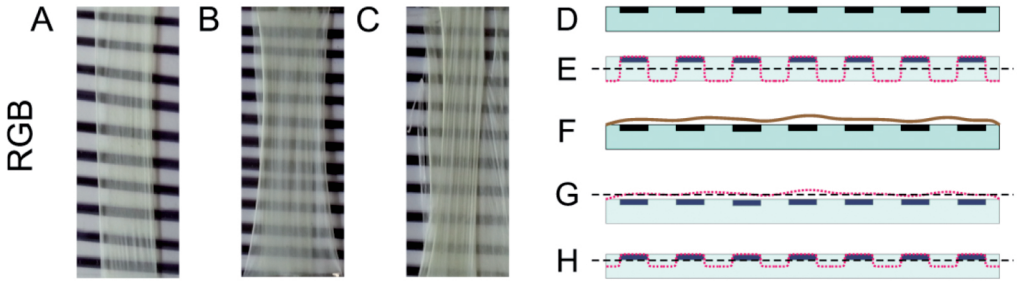

Fig. 2: Experimental setup for the evaluation of the penetration depth. A to C show an RGB image of the different numbers of epidermal layers (one to three). D and E represent the profile of the microscope slide with the stripe pattern and the theoretic scanning result without an epidermal layer, respectively. F to H show the case with one epidermal layer and two possible scanning results. The dashed line represents the best-fit plane.

the control pattern anymore, suggesting that the received signal is backscattered on top of or inside the second epidermal layer.

To compare the results to the finding of Paulus et al. (2014c), where the exposure time had a significant impact on the measured penetration depth, the epidermal stripes were scanned using different exposure times varying from 0.35 ms to 0.8 ms. As illustrated in Fig. 4A, B, for the red laser sensor, the measured pen-

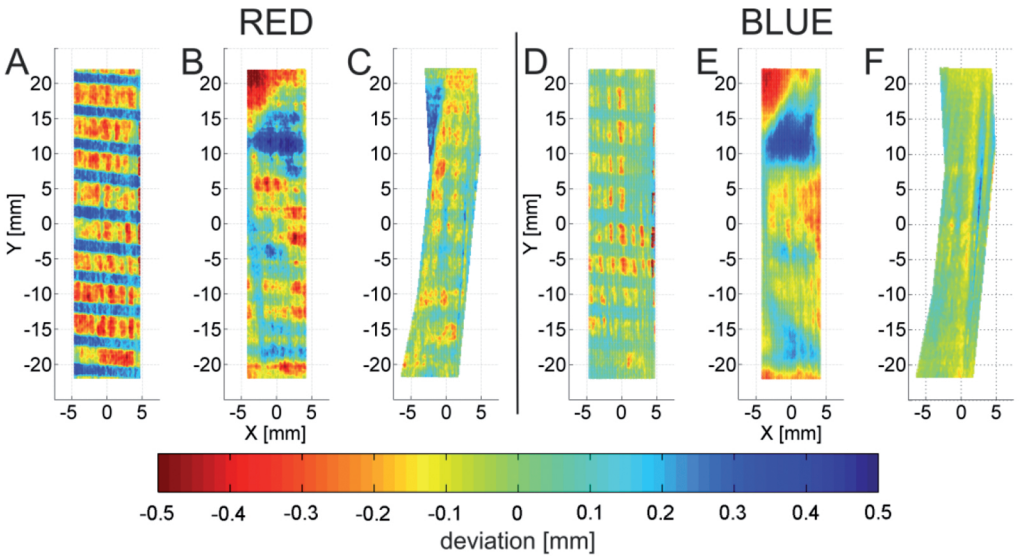

Fig. 3: Evaluation of the penetration of the red and the blue laser scanner at a constant exposure time. All point clouds were rotated to the x-y-plane and coloured using the deviation from the best-fit plane. A to C illustrate the coloured point cloud for one, two and three epidermal layers measured with the red and D to F measured with the blue scanner, respectively.

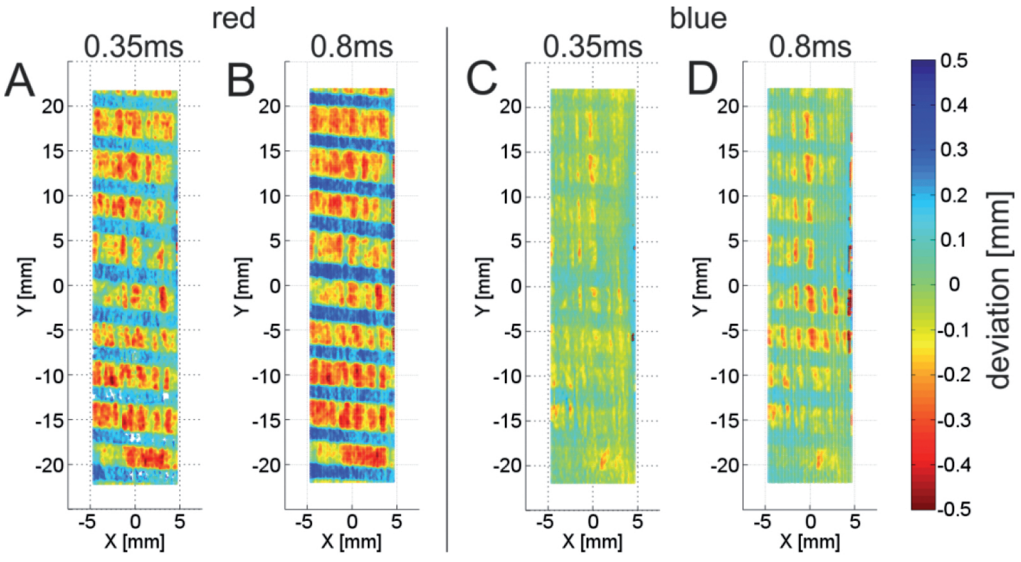

Fig. 4: Deviations from the best-fit plane for one epidermal stripe using the red and the blue laser sensors at different exposure times.

etration depth was slightly increased when scanning with longer exposure times, which is apparent from the larger deviations from the best-fit plane. A similar but slightly weaker effect was achieved for the blue laser sensor (Fig. 4C, D).

To explain this effect the physical shape of the backscattered laser line has to be taken into account. Due to a constant luminous power of the emitted laser, the physical penetration depth should be constant depending on the wavelength (Barolet 2008). However, in case of semi-transparent materials, like the epidermis, the signal originating inside the surface structure is weakened. The exposure time controls the amount of backscattered laser light that is collected by the CCD-array elements. In other words, the longer the exposure time, the more light is collected. As a consequence, when longer exposure times are used, the weakened signal originating from inside the surface structure is additionally collected by the CCD-array and the centre of gravity of the received laser line is displaced. This displacement results in a longer distance measurement (Dupuis & Kuhlmann 2014) and, therefore, in a larger measured penetration depth.

3.2 *Measuring Photoactive Plant Tissues*

In a second experiment the impact of the chlorophyll located in the mesophyll layer on the laser measurements was investigated. To simulate measurements of the mesophyll layer without any impact of cuticle and epidermis, pieces of filter paper were soaked with different concentrations of leaf pigments extracted from sword fern leaves (*Nephrolepis exaltata* (L.) Schott). The pieces were arranged in order visually by colour, measured with both laser sensors and the actual chlorophyll (type a and b) as well as carotenoid concentrations were determined after extraction with 10 ml of 80% acetone as described in Porra et al. (1989).

The impact of the leaf pigments on the received signal was determined by analysing the intensity values obtained for each 3D point. Therefore, the regions of the paper pieces were extracted manually from the point cloud using MATLAB® 2009b (The MathWorks Inc., Natick, MA, USA). To overcome possible variations of the chlorophyll distribution inside the filter paper, one intensity value for each region representing the averaged intensity for all points inside the region was determined for data analysis.

Fig. 5 shows an RGB image and the results of the experiment. To compensate the different physical power of both lasers (8 mW for the blue laser *vs.* 10 mW for the red), we chose different exposure times (0.75 ms for the red and 1.25 ms for the blue laser) to obtain nearly the same averaged intensity at the lowest chlorophyll concentration.

Regarding the colour coded point clouds in Fig. 5, as expected, both sensors interacted with chlorophyll. With an increasing chlorophyll content from 5.8 up to 24.7 µg·cm^{-2} (first ten stripes: A-1 to A-7 and B-1 to B-4) both laser colours provided a linear decreasing trend ($R^2 > 0.95$) with nearly the same slope of -2.8%·cm^2·µg^{-1} for the blue laser and of -2.6%·cm^2·µg^{-1} for the red one (Fig. 6).

In case of higher concentrations, a break can be found in the linear function and both sensors exposed a slightly different behaviour.

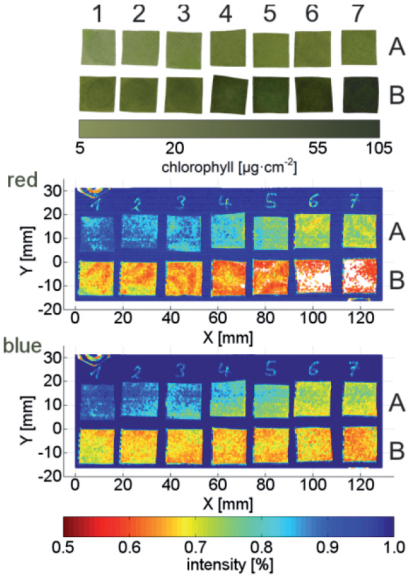

Fig. 5: Investigation of the interaction of extracted chlorophyll ($chl_A + chl_B$) with the laser of both laser scanners. The chlorophyll content ranged from 5.8 µg·cm^{-2} up to 102 µg·cm^{-2}.

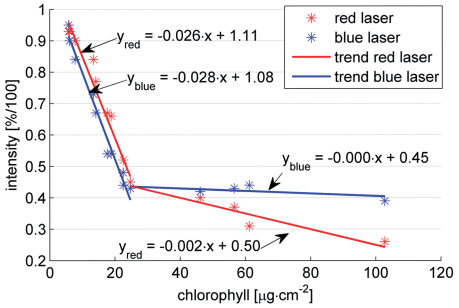

Fig. 6: Decrease of the intensity with an increasing chlorophyll content.

While the intensity of the red laser was still decreasing with a much smaller slope, the intensity of the blue sensor remained approximately constant (B-5 to B-7). This difference could probably be linked to the different physical penetration depths of the two lasers. As already shown in the previous experiment, the physical penetration depth of the blue laser is smaller compared to the red one. This leads to the assumption that the blue laser interacted with chlorophyll in the upper layers of the filter paper, while the red laser penetrated deeper into the filter paper. This resulted in an interaction with more chlorophyll and therefore to a stronger relative absorption.

4 Discussion

Transferring the results of sections 3.1 and 3.2 to a real plant surface leads to the following assumptions:

Scanning with the red laser wavelength (658 nm) enables the sensor to penetrate the leaf surface and to interact with deeper plant tissues. This interaction leads to the partial absorption of the emitted laser ray by the chlorophyll located in the mesophyll layer and therefore to lower intensity values. Thus, the derived point cloud should provide a higher measurement noise, caused by the low intensity of the signal, and should be systematically displaced, because the signal is backscattered in the mesophyll layer.

Using the blue laser wavelength (405 nm) should lead to different result. Due to the smaller physical penetration depth the laser should at best not be able to interact with the chlorophyll, which in turn results in a chlorophyll-independent intensity. This should result in a lower measurement noise without a systematic displacement, i.e. the geometric accuracy is higher compared to the red one.

Nevertheless, analysing the intensity of the red laser sensor should increase the interpretability of the point cloud because variances in the chlorophyll content should alter the measured intensity values.

5 Possible Applications

In this section the results obtained in section 3 are transferred to real plants and possible applications are presented, where the intensity of the received signal can be used to characterize the physiology of the plant.

5.1 *Stages of Leaf Senescence*

In the first application we present how the intensity of the received signal is affected by the different stages of leaf senescence. Therefore, leaves of bottlebrush buckeye (*Aesculus parviflora* Walter) containing areas with different stages of leaf senescence ranging from healthy (green) to chlorotic (yellow) and necrotic (brown) tissues (Fig. 7A) were scanned. We expected the different stages to result in different intensity values in case of a penetration of the laser line into the mesophyll layer.

Using the red laser sensor, chlorotic and necrotic areas of the bottlebrush buckeye leave caused different intensity values, due to changes in chlorophyll concentration. Healthy areas with higher chlorophyll content resulted in lower intensity values, while chlorotic and necrotic regions provided higher intensity values (Fig. 7B).

A different result was achieved when scanning with the blue laser. Changes in chlorophyll content were not visible in the intensity distribution, what implies that the received signal originated on top of the leaf surface and the measured penetration depth was minimized. This in turn leads to a higher geometric accuracy.

Compared to classical photogrammetric approaches where the stages of leaf senes-

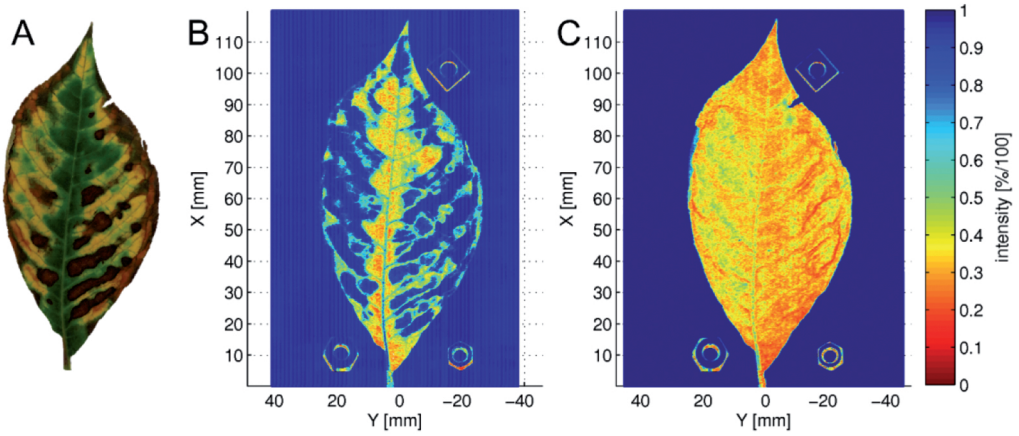

Fig. 7: The leaf of a bottlebrush buckeye (A) was scanned with both laser scanners. The resulting point clouds were rotated to the x-y-plane and coloured according to the intensity values (red laser: B, blue laser: C).

cence can be easily identified using the RGB values, the laser measurements provide a direct and highly accurate access to the 3D geometry of the plant or a leaf. Photogrammetric approaches using Structure from Motion (SfM) and Multi View Stereo (MVS) also enable the reconstruction of coloured 3D point cloud from digital images (Paproki et al. 2012, Rose et al. 2015). However, these approaches provide lower point densities and also a lower geometric accuracy.

Using laser scanning and the intensity of reflection enables an easy and accurate way to get access to the 3D structure and the stage of leaf senescence of single plant organs.

5.2 *Detection of Plant Diseases*

The detection of plant diseases is of high relevance in plant research. The integration of the detection by non-invasive sensors in an automated canopy measurement process or in a high-throughput phenotyping approach would support agricultural praxis and breeding processes (Mahlein et al. 2012a).

In this experiment, we illustrate how the intensity values can support a detection of diseased leaf areas. Therefore, norway maple leaves (*Acer plantanoides* L.) diseased with powdery mildew (*Sawadaea tulasnei* (Fuckel) Homma 1937) were scanned at a fixed exposure time and analysed based on the resulting intensity values. Because powdery mildew modifies the leaf surface in terms of colour and structure, it should thus change the reflective properties. Fig. 8 shows the pattern of damage caused by powdery mildew in a microscope RGB image and semi-thin sections of the leaf surface, prepared and observed

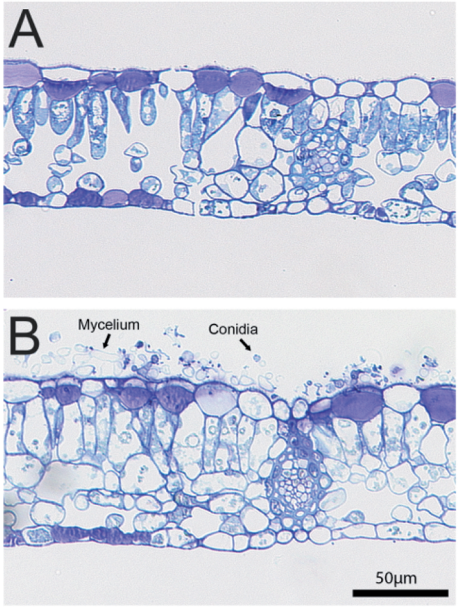

Fig. 8: Semi-thin sections of healthy (A) and diseased (B) plant tissues of a maple leaf.

with a photomicroscope according to Mahlein et al. (2012b).

It can be observed from Fig. 8B that the mycelium and the conidia of the fungus alter the rather smooth surface structure in an irregular way. Thus, the emitted laser is backscattered at the rough surface in several directions which is similar to a diffuse reflection, e.g. provided by commercial coating spray. For this reason, we expected higher intensity values at the diseased regions and a lower intensity at the healthy regions.

For the quantification of the disease severity the ratio of diseased and healthy leaf area was calculated by a basic threshold. The point cloud was projected into the x-y-plane and every point was assigned to one pixel in order to generate a 2D greyscale image. Due to the flat attachment of the leaf to the x-y-plane and the vertical alignment of the laser plane, the uncertainties caused by the projection are quite small. In the greyscale image the leaf was manually extracted from the background and the infected pixels were estimated using a threshold value. The disease severity in % was calculated from the estimated amount of diseased pixels in relation to the total amount of leaf pixels.

The results of the threshold approach were compared to manually labelled data of RGB images using the free image processing software GIMP (GIMP 2.8.6, www.gimp.org).

The coloured point clouds illustrated in Fig. 9B, C confirm the theoretical assumption. Regions diseased by powdery mildew provide much higher intensity values compared to healthy regions. The quantification of the relative disease severity using an empirically chosen threshold value of x = 200 which corresponds to an intensity value of ~79%, resulted in a relative disease severity of 38%, compared to 40% manually labelled by an expert. The difference could be addressed to uncertainties in the manual labelling process.

Due to the higher intensity values, diseased regions provide a lower local measurement noise. By combining these spatial features together with the intensity (as a spectral feature) and by using a more complex machine learning approach such as support vector machines, an automated and more precise classification should be possible.

In contrast to the results presented in section 5.1, both laser colours showed nearly the same intensity distribution and the powdery mildew diseased leaf areas were visible for both scanners (Fig. 9B, C). This behaviour can be addressed to the fact that powdery mildew changes the structure of the leaf surface as shown in Fig. 8B.

However, taking a closer look at the intensity distributions of both scanners, some differences can be detected regarding the main and smaller leaf veins. In the intensity image of the red laser sensor (Fig. 9B) the main leaf vein and some smaller veins were imaged with high intensity values (~90%) due to lower chlorophyll content. A different result was obtained from the blue scanner. Small leaf veins were not visible in the intensity image

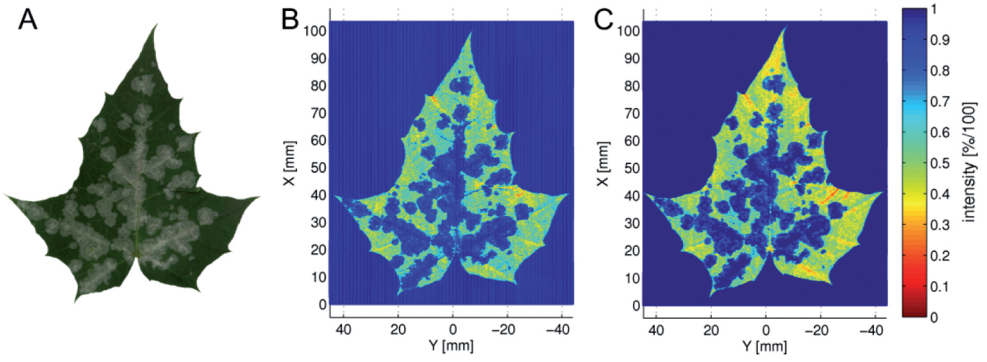

Fig. 9: Detection of the mildew infection of a maple leaf (RGB image: A). The point clouds of the red (B) and the blue (C) laser scanner were rotated to x-y-plane and coloured using the intensity values.

and the main leaf vein was imaged with a low intensity (~50%). This leads to the assumption that the principle behaviour is the same as obtained in the previous experiments. However, powdery mildew changes the reflective properties of the leaf surface in a way that it can be identified with both laser colours.

Summing up, this experiment pointed out that the parameter intensity of reflection supports the detection of plant diseases like powdery mildew without using additional sensors like RGB- or hyperspectral cameras. The simple approach using a threshold to identify infected regions illustrated the significance of the intensity values for plant analysis.

6 Conclusion

Using two commercial state-of-the-art 3D laser triangulation sensors with different wavelengths (658 nm and 405 nm) and providing the intensity of the received signal as additional measuring information gives a great advantage for the metrological and functional analysis of plant measurements. Systematic deviations caused by penetration of the laser into the leaf's surface were found for the red laser sensor, while the blue laser sensor was able to measure the real surface of the plant. Thus, from a metrological viewpoint the blue laser sensor provides higher geometric accuracy. However, despite the lower geometric accuracy, using the intensity values of the red laser sensor measured for every 3D point uncovers detailed and highly resolved information about changes of the stage of leaf senescence, tissue content or plant diseases. Thus, a combination of these laser wavelengths enables a precise imaging of the 3D surface structure of plants together with an analysis of the underlying surface tissues. As we used commercial 3D scanning systems, our experimental results can directly be transferred to existing phenotyping platforms using similar laser scanning systems.

Acknowledgements

The authors also want to express their gratitude to Birgit Kretschmann for proofreading the manuscript. This work could be carried out due to the financial support of the German Federal Ministry of Education and Research (BMBF) within the scope of the competitive grants program "Networks of excellence in agricultural and nutrition research – CROP. SENSe.net" (Funding code: 0315529).

JD, SP, TE, AKM and HK designed the study. JD, SP and TE interpreted the measured data and drafted the manuscript. Measuring and programming was carried out by JD and SP. Extracting the chlorophyll and analysing its content in the filter paper was performed by TE. The microscope images and the profiles of the leaf surfaces were prepared and analysed by AKM. HK directed the research and gave initial input. All authors read and approved the final manuscript.

References

Barolet, D., 2008: Light-Emitting Diodes (LEDs) in Dermatology. – Seminars in Cutaneous Medicine and Surgery **27** (4): 227–238.

Bellasio, C., Olejníčková, J., Tesař, R., Šebela, D. & Nedbal, L., 2012: Computer reconstruction of plant growth and chlorophyll fluorescence emission in three spatial dimensions. – Sensors **12** (1): 1052–1071.

Donges, A. & Noll, R., 1993: Lasermeßtechnik. Grundlagen und Anwendungen. – Hüthig Verlag, Heidelberg.

Dupuis, J. & Kuhlmann, H., 2014: High-Precision Surface Inspection: Uncertainty Evaluation within an Accuracy Range of 15µm with Triangulation-based Laser Line Scanners. – Journal of Applied Geodesy **8** (2): 109–118.

Fiorani, F., Rascher, U., Jahnke, S. & Schurr, U., 2012: Imaging plants dynamics in heterogenic environments. – Current Opinion in Biotechnology **23** (2): 227–235.

Gordon, B., 2008: Zur Bestimmung von Messunsicherheiten terrestrischer Laserscanner (Doctoral Dissertation). – Technische Universität Darmstadt.

Honsdorf, N., March, T.J., Berger, B., Tester, M. & Pillen, K., 2014: High-throughput phenotyping to detect drought tolerance QTL in wild barley introgression lines. – PloS One **9** (5): e97047, doi: 10.1371/journal.pone.0097047.

Mahlein, A.-K., Oerke, E.-C., Steiner, U. & Dehne, H.-W., 2012a: Recent advances in sens-

ing plant diseases for precision crop protection. – European Journal of Plant Pathology **133** (1): 197–209.

Mahlein, A.-K., Steiner, U., Hillnhütter, C., Dehne, H.-W. & Oerke, E.-C., 2012b: Hyperspectral imaging for small-scale analysis of symptoms caused by different sugar beet diseases. – Plant Methods **8** (1): 3, doi: 10.1186/1746-4811-8-3.

Mikhail, E.M. & Ackermann, F.E., 1976: Observations and least squares. – IEP-A Dun-Donnelley Publisher, New York, NY, USA.

Mustafa, F.H. & Jaafar, M.S., 2012: Comparison of wavelength-dependent penetration depths of lasers in different types of skin in photodynamic therapy. – Indian Journal of Physics **87** (3): 203–209.

Næsset, E. & Bjerknes, K.-O., 2001: Estimating tree heights and number of stems in young forest stands using airborne laser scanner data. – Remote Sensing of Environment **78** (3): 328–340.

Omasa, K., Hosoi, F. & Konishi, A., 2007: 3D lidar imaging for detecting and understanding plant responses and canopy structure. – Journal of Experimental Botany **58** (4): 881–898.

Paproki, A., Sirault, X., Berry, S., Furbank, R. & Fripp, J., 2012: A novel mesh processing based technique for 3D plant analysis. – BMC Plant Biology **12:** 63.

Paulus, S., Dupuis, J., Mahlein, A.-K. & Kuhlmann, H., 2013: Surface feature based classification of plant organs from 3D laserscanned point clouds for plant phenotyping. – BMC Bioinformatics **14:** 238.

Paulus, S., Behmann, J., Mahlein, A.-K., Plümer, L. & Kuhlmann, H., 2014a: Low-Cost 3D Systems: Suitable Tools for Plant Phenotyping. – Sensors **14** (2): 3001–3018.

Paulus, S., Dupuis, J., Riedel, S. & Kuhlmann, H., 2014b: Automated Analysis of Barley Organs Using 3D Laser Scanning: An Approach for High Throughput Phenotyping. – Sensors **14** (7): 12670–12686.

Paulus, S., Eichert, T., Goldbach, H.E. & Kuhlmann, H., 2014c: Limits of Active Laser Triangulation as an Instrument for High Precision Plant Imaging. – Sensors **14** (2): 2489–2509.

Paulus, S., Schumann, H., Kuhlmann, H. & Léon, J., 2014d: High-precision laser scanning system for capturing 3D plant architecture and analysing growth of cereal plants. – Biosystems Engineering **121:** 1–11.

Pfeifer, N., Gorte, B. & Winterhalder, D., 2004: Automatic reconstruction of single trees from terrestrial laser scanner data. – 20th ISPRS Congress: 114–119, Istanbul, Turkey.

Porra, R.J., Thompson, W.A. & Kriedemann, P.E., 1989: Determination of accurate extinction coefficients and simultaneous equations for assaying chlorophylls and extracted with four different solvents: verification of the concentration of chlorophyll standards by atomic absorption spectroscopy. – Biochimica et Biophysica Acta (BBA)-Bioenergetics **975** (3): 384–394.

Rose, J., Paulus, S. & Kuhlmann, H., 2015: Accuracy Analysis of a Multi-View Stereo Approach for Phenotyping of Tomato Plants at the Organ Level. – Sensors **15** (5): 9651–9665.

Strothmann, W., Ruckelshausen, A. & Hertzberg, J., 2014: Multiwavelength laser line profile sensing for agricultural crop characterization. – SPIE Photonics Europe: 91411K–91411K.

Wagner, B., Gärtner, H., Ingensand, H. & Santini, S., 2010: Incorporating 2D tree-ring data in 3D laser scans of coarse-root systems. – Plant and Soil **334** (1–2): 175–187.

Wahabzada, M., Paulus, S., Kersting, K. & Mahlein, A.-K., 2015: Automated interpretation of 3D laserscanned point clouds for plant organ segmentation. – BMC Bioinformatics **16:** 248.

Wei, G., Shalei, S., Bo, Z., Shuo, S., Faquan, L. & Xuewu, C., 2012: Multi-wavelength canopy LiDAR for remote sensing of vegetation: Design and system performance. – ISPRS Journal of Photogrammetry and Remote Sensing **69:** 1–9.

Addresses of the Authors

M.Sc. Jan Dupuis & Prof. Dr.-Ing. Heiner Kuhlmann, Universität Bonn, Institut für Geodäsie und Geoinformation, Nussallee 17, D-53115 Bonn, Tel.: +49-228-733571, Fax: +49-228-732988, e-mail: {dupuis}{kuhlmann}@igg.uni-bonn.de

Dipl.-Inform. Stefan Paulus, LemnaTec GmbH, Pascalstr. 59, D-52076 Aachen, e-mail: stefan.paulus@lemnatec.de

Dr. Anne-Katrin Mahlein, Universität Bonn, Institut für Nutzpflanzenwissenschaften und Ressourcenschutz, Abteilung Phytomedizin, Meckenheimer Allee 166a, D-53115 Bonn, e-mail: amahlein@uni-bonn.de

PD. Dr. Thomas Eichert, Universität Bonn, Institut für Nutzpflanzenwissenschaften und Ressourcenschutz, Abteilung Pflanzenernährung, Karlrobert-Kreiten-Str. 13, D-53115 Bonn, e-mail: t.eichert@uni-bonn.de

Manuskript eingereicht: September 2015
Angenommen: Oktober 2015

PFG 2015 / 6, 0449–0456
Stuttgart, December 2015

Article

Development of an ISO-Standard for the Preservation of Geospatial Data and Metadata: ISO 19165

Wolfgang Kresse, Koszalin, Poland & Joan Masó Pau, Barcelona, Spain

Keywords: long-term preservation, archiving, geospatial data, ISO, OGC, metadata

Summary: Most of the paper maps produced a century ago are still very accessible in cartographic libraries preserved by the producer. It is our present obligation to guarantee the preservation of digital geospatial data today and allow for digital cartographic accessibility one century into the future. In addition, there is an increasing demand for older maps that goes beyond pure historical interest motivated by the study of dynamic problems such as impacts of the climate change, human activities and sustainability. The long-term preservation of large volumes of geospatial data in a uniform way still remains an unsolved question. A systematic solution has been demanded by National Mapping and Archival Agencies in Europe and North America. One year ago the ISO/TC 211 "Geographic information / Geomatics" published a New Work Item Proposal (NWIP) named ISO 19165 "Preservation of digital data and metadata" accompanied by a Working Draft document. The proposed standard is built upon the principles laid down in the ISO 14721 "Open Archival Information Systems" and upon the data model of the ISO 19115-1 "Metadata – Part 1: Fundamentals". This article reports on the specialization of both standards for the purpose of archiving of geospatial data and asks for contributions to the ISO 19165 under development.

Zusammenfassung: *Entwicklung einer ISO-Norm für die Archivierung von Geodaten: ISO 19165.* Papierkarten aus dem frühen 20. Jahrhundert sind meist heute noch gut zu gebrauchen. Inwieweit man digitale Geodaten von heute in 100 Jahren nutzen kann, bleibt abzuwarten. Zudem ist ein gestiegener Bedarf an historischen Karten zu beobachten. Die Langzeitarchivierung von umfangreichen Geodaten in einheitlicher Form bleibt vorerst eine ungelöste Aufgabe. Eine systematische Lösung wurde von nationalen Vermessungsbehörden und Archiven in Europa und Nordamerika gefordert. Vor einem Jahr veröffentlichte daher das ISO/TC 211 „Geographic information / Geomatics" ein New Work Item Proposal (NWIP) unter dem Namen ISO 19165 „Preservation of digital data and metadata" verbunden mit einem bereits fertiggestellten Working Draft Dokument. Die neue Norm baut auf den in der ISO 17421 „Open Archival Information System" dargelegten Prinzipien und dem Datenmodell der ISO 19115-1 „Metadata – Part 1: Fundamentals" auf. Dieser Beitrag berichtet von der Spezialisierung der beiden ISO-Normen für Zwecke der Archivierung von Geodaten und ruft zur Beteiligung bei der weiteren Entwicklung der ISO 19165 auf.

1 Introduction

Looking back a century, or even before, we find a lot of geographic information created at that time that is still accessible and usable in the form of paper maps. Paper has proved itself a good medium for long term preservation if it is looked after with appropriate care. It is easy to handle and printed information in graphical form is immediately accessible. However, in today's digital world, geographic information is produced and distributed predominantly in digital formats that have a very strong reliance on technology to both store and access data. If we look one century ahead it is quite difficult to see how the preservation of digital data will be assured and how the information we generate today will be accessed (Rönsdorf et al. 2013).

In addition, there is increasing demand for older and superseded data to support historical and temporal analyses related to change in Earth's natural and human landscape (Library of Congress 2010), to know the im-

www.schweizerbart.de
DOI: 10.1127/pfg/2015/0000
1432-8364/15/0000 $ 2.00

pact of human activities and eventually to extract lessons for a sustainable development that does not go irreversibly beyond planetary boundaries (Steffen et al. 2015). The exponential growth of studies done as a result of the free availability of the complete Landsat series is another example of the monetary value of well preserved Earth observation archives (Wulder et al. 2012). Consequently, national mapping agencies and Earth observation data producers (including remote sensing space agencies and in-situ campaigns) are challenged to preserve the history of geospatial data before new updates take place.

After some years of a short history of geospatial digital production, we are now realising that long-term preservation of large digital geospatial datasets in a uniform way is a still unsolved question. Though the problem has been known for a while it has been mitigated by producer's comprehensive storage policies and, so far has been compensated by the fast development of storage media towards cheap and voluminous units. However, currently the growth of data is faster than the growth of storage media, particularly due to constant inputs to remote sensing datasets.

Remote sensing agencies have realized this issue and they already had applied data preservation policies and procedures to their data archives. The European Space Agency (ESA) Preserved Data Set Content (LTDP 2012) and the NASA Earth Science Data Preservation Content Specification (NESDPCS 2012) are two examples of success stories in the remote sensing community. A systematic solution has been demanded also by National Mapping and Archival Agencies in Europe and North America. In 2003 the International Organization for Standardization (ISO) published a first preservation standard developed by a group of agencies running imaging space-borne sensors: the ISO 14721 "Open Archival Information System" (OAIS). Though the document was developed by space agencies, the specification is generic enough and has been applied to digital libraries around the world.

Solutions commonly applied in libraries to preserve printed documents (including OAIS) cannot be directly applied because geospatial data possesses a number of peculiarities that do not agree with or even contradict common archival principles. Some of the data are never final like cadastral data and thus in principle could never be archived. Other data has legal or ownership restrictions which keep their validity and must be acknowledged by an archive. Topologically structured data features are fully interlinked and thus cannot be separated into packages without modifying their structure. Geospatial Information Systems design principles often force the data models to be divided into thematic layers and each one considering geospatial data, metadata, symbolization, printing, etc. that are often stored individually. In addition, geospatial data are often linked with non-geospatial information increasing the storage capacities even more. Service-Oriented Architectures (SOA) produce maps on-the-fly sometimes related with highly dynamic real time phenomena which are gone shortly after the call, thus, hardly impossible to be preserved. Though some of the cases may rarely require archival, in others can open new forms of studying human evolutions. For example, the CartoBD company is storing all georeferenced twits believing that they will allow for studies of human activities in the future. These emerging cases illustrate the differences and potentialities that archival of digital geospatial data can provide. The authors assume that a preservation case for every example could be perceived. Finally, large data volumes of the imagery domain tend to exhaust the available long-term storage capacities.

The ISO/TC 211 "Geographic information / Geomatics" is ISO's Technical Committee that pools all standardization projects for geographic information. This is the reason why the national mapping agencies of Europe, the Open Geospatial Consortium and others have asked ISO/TC 211 to take the action. Though several other topics have been standardized already, an ISO-standard that addresses the specificities of the preservation of geospatial information is still missing. Many works of administrative units require ISO-standard as a fundament while non-ISO-standard are not accepted e.g. for calls for tenders, in particular in the U.S..

The development of the ISO 19165 "Preservation of geospatial data and metadata" has started a year ago. In June 2015, the project

team discussed the first Working Draft which is built upon the ISO 14721 and a proposal of the Open Geospatial Consortium. This proposal was prepared by the Catalan Cartographic and Geologic Institute aiming at the definition of a minimum set of metadata for preservation by extending the existing ISO 19115-1 "Metadata – Part 1: Fundamentals".

The intention of this article is disseminate the work that the ISO/TC 211 is doing to cover the need of a geospatial preservation standard toward a future official ISO 19165.

2 Preliminary Works

The most detailed standard that addresses preservation in a generic way is the ISO 14721 "Open Archival Information System". This ISO standard has been initiated by the NASA and developed in cooperation with the ESA and other space agencies (ISO 14721:2012). A fundamental element of this ISO-standard is the Information Package (IP) which contains the data (content information) together with their metadata (preservation description information). This concept has been adopted by the new ISO 19165. The definition of new metadata elements will be restricted to those not already defined in the ISO 19115-1.

The European National Mapping and Cadastral Agencies published 16 principles for the archival of geospatial data under the title GI+100 (Rönsdorf et al. 2013). Four important principles sound:

- Archiving of digital Geographic Information begins at the point of data creation, rather than at the point of withdrawal from active systems (1).
- Be selective and decide what to archive and what to lose (3).
- Consider preservation timeframes of 1, 10, 100 years (4).
- Geographical data should be preserved in a way that non geo-specialists can handle (8).

In a similar way the U.S. Library of Congress (2010) demands appraisal and selection of geospatial data because of the limited resources that most organizations have for preservation.

An international group of library experts published under the leadership of the U.S. a data dictionary for preservation of metadata, the PREMIS data model (PREMIS 2012). Ramapriyan & Moses (2012) prepared the data preservation content specification of NASA's Earth sciences division. The U.S.-states North Carolina, Kentucky, Montana, Utah, started together with the Library of Congress GeoMAPP in 2010. The GeoMAPP effort aimed to address the preservation of "at risk" digital geospatial content such as land parcels, zoning, roads, and jurisdictional boundaries which change regularly. Existing copies of these data are often at risk of being overwritten when updates or changes are made (GeoMAPP 2010). Higgins (2008) presented a Curation Lifecycle Model developed at the Digital Curation Centre of the University of Edinburgh, United Kingdom. Engel et al. (2013) of the land survey administration of Baden-Württemberg, Germany, discuss the archival with a focus on appropriate data formats. A methodology for the preparation of documentation evaluation and access proposals (PAAD) is prepared by the Catalonian National Commission on Access, Evaluation and Selection of Documents (CNAATD 2015).

A broad discussion on aspects of the preservation of digital cartography can be found in Jobst & Gartner (2011). Moe & Longhenry (2013) discuss technical aspects of the preservation of the USGS aerial film archive.

3 Working Draft ISO 19165

Since the year 2010 a group of the European National Mapping and Cadastral Agencies requested an ISO-standard for the preservation of geospatial data. The National Standardization Body of Germany (DIN) prepared a New Work Item Proposal that was accompanied by a Working Draft document. In the autumn of 2014 the members of the ISO/TC 211 "Geographic information / Geomatics" approved the new project with no no-votes. This was an indication of the strong demand for ISO-standard, now numbered ISO 19165.

3.1 *Scope*

According to the scope-section this standard sets the rules for the long-term preservation of digital geospatial data. These data include metadata and other ancillary data that are necessary to fully understand and rebuild the archived digital environment.

Geospatial data are preserved as a geospatial archival information package. This standard defines its details. A geospatial archival information package will be fully self-explanatory and will allow a future reconstruction of the dataset without external documentation.

3.2 *Terms and Definitions*

The first Working Draft contains 37 terms and definitions that were mostly adopted from the ISO 14721 "OAIS" and the ISO 19115-1 "Metadata – Part 1: Fundamentals".

3.3 *Summary of the ISO 14721*

The Information Package (IP) is central to the OAIS. The standard distinguishes further between: the input, the Submission Information Package (SIP); the storage, the Archival Information Package (AIP); and the output, the Dissemination Information Package (DIP) (Fig. 1). It does not provide any implementation or format for the IP.

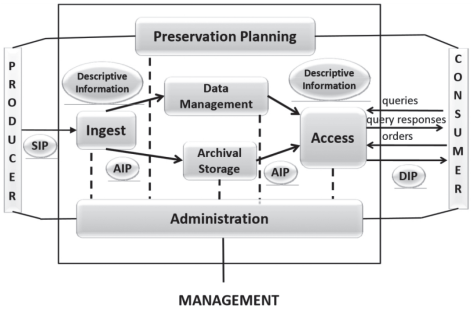

Fig. 1: Model of the Open Archival Information Standard (OAIS). SIP = Submission Information Package, AIP = Archival Information Package, DIP = Dissemination Information Package (ISO 14721:2012).

In addition, the ISO 14721 defines a number of responsibilities of the organization that operates an OAIS archive. Those include a sufficient control of the information needed to ensure long-term preservation, as well as copyright implications, intellectual property and other legal restrictions.

Every archive needs a designated community which is able to understand the archived information without needing special resources, such as the ones available to the experts who produced the information.

No matter how well an OAIS maintains its current holdings, it will eventually need to migrate much of its holding to different media. Digital migration is defined to be the transfer of digital information, while intending to preserve it.

Three major motivators are seen to drive digital migration of AIPs within an OAIS. These are:

- Improved cost-effectiveness: The rapid pace of hardware and software evolution provides greatly increasing storage capacities and transfer bandwidths at reducing costs
- New consumer-service requirements
- Media decay

3.4 *Preservation Principles of the ISO 19165*

3.4.1 Prioritization

The exponential growth of the data volume prevents a full archival of all data. Consequently, only a selected subset can go for a long-term archive. A temporal classification may follow the proposed categories 1 year, 10 years, and 100 years.

3.4.2 Data formats

Today, all geospatial data are stored in commonly accepted specialized data formats. Those formats have a specific structure and include metadata. Some of the formats are standardized by ISO and/or IEC (International Electrotechnical Commission), others are de-facto standards. In 2014, the format description document (FDD) database of the US Congress Library contained 334 format de-

scriptions, 34 of them are geospatially related (Library of Congress 2011). A more comprehensive list of formats can be found in the GDAL/OGR read and conversion open source libraries (GDAL 2015).

It is almost impossible to recommend a subset of formats since each format is used in its context. Instead, a geospatial dataset should be archived together with a fully documented data format specification. For practical reasons the documentation of the data format can be delegated to a format-registry.

3.4.3 Database

Many geospatial data are object-structured and stored in databases (sometimes known as geodatabases). In order to preserve this structure, the full database content should be transferred to the archive, which demands an archiving strategy that allows a persistent understanding of the technology for accessing this dataset.

3.4.4 Properties of geospatial data

Geospatial data often have a large number of attributes of which only a few are relevant for a specific mapping product. For instance, a 1:100,000 map does not show most of the road details, such as traffic lights. In the case of a limited archival space, this observation leads to another method of data reduction: assumptions about the future potential use of the data. Based on this assumption, a decision is needed which of the properties and which of their details will be archived or dropped. As a result, not all properties of the geospatial data are archived. Only those are maintained which are required to create one of the assumed products.

3.4.5 Level of aggregation

Often the same geospatial data exists at several servers with different levels of aggregation and processing. This means that prior to archiving it needs to be specified which levels of detail are required for archival. In some cases, raw data could be too dependent on the sensor technology or software licenses, and a further elaborated product could be easier to use and better for storage. In other cases, aggregated products can be derived from raw data with no or with little costs. Then, preserving the processing algorithms with the raw data could be the right choice.

3.4.6 Gold copy

The totality of all methods can never guarantee a full recovery of the data after a very long period of time. In order to increase reliability, a separate copy version of the 100 year data preservation should be established in an open format, file based repositories, avoiding databases, or other complex environments. Often, this copy is called a gold copy.

3.4.7 Intellectual Property Rights

As mentioned in the introduction, the regard of intellectual property rights imposed on the data is crucial. Authoritative geospatial data often possess legal restrictions that are written in license agreements. Licences for geospatial data usage need to include a special clause authorizing future curators the rights for preservation actions including archive, media migration and redistribution among future users of the archived data.

3.4.8 Time

According to an archiving rule the incoming data should have lost their relevance for the governmental work. However, many geospatial data are never obsolete or are continuously updated such as cadastral data. These kinds of geospatial datasets never become mature for archiving. The ISO 19165 defines a number of methods to overcome this problem.

3.4.9 Archiving package for geospatial data registries

The standard should define, as one of its central components, the elements of the AIP. This package should be ready to be shared with other organizations, including those outside the geospatial community. Studies or other forms of research are needed to find out the user's requirements.

The packaging format should be built upon existing standards. During the first project team meeting an example was presented: the Open Packaging Convention defined by Microsoft. This packaging format is standardized as ISO 29500-2 and ECMA-376 and it has a reference implementation in the geospatial world (MMZX format) introduced in the MiraMon GIS.

The ISO 19165 will define specialized versions of the IPs named Geo-SIP, Geo-AIP, and Geo-DIP. Their special properties include, lossless compression, cartographic series support (a manageable regional size, e.g. series of tiles of 10 km x 10 km), and a container for information regarding geometry (vector and raster), attributes, topology, metadata, quicklooks and recommendation on how to symbolize the data.

3.5 *Metadata built upon ISO 19115-1*

A geospatial dataset is always linked to a set of metadata. The metadata should be archived in a way that allows an undoubtedly reference between both data and metadata. Preservation requires that more emphasis is put on metadata. In the long term, when the producer of the dataset is no longer available metadata could become almost the only source of additional information about the preserved dataset.

A number of metadata models have already been proposed for the preservation of geospatial data such as the well-known prototyped PREMIS metadata model. It defines entities, among which are Intellectual entity (intellectual property of the dataset), Digital Objects (dataset), Agents (person or organization involved in the life of the dataset), and Rights (permissions pertaining to the dataset) (PREMIS 2012).

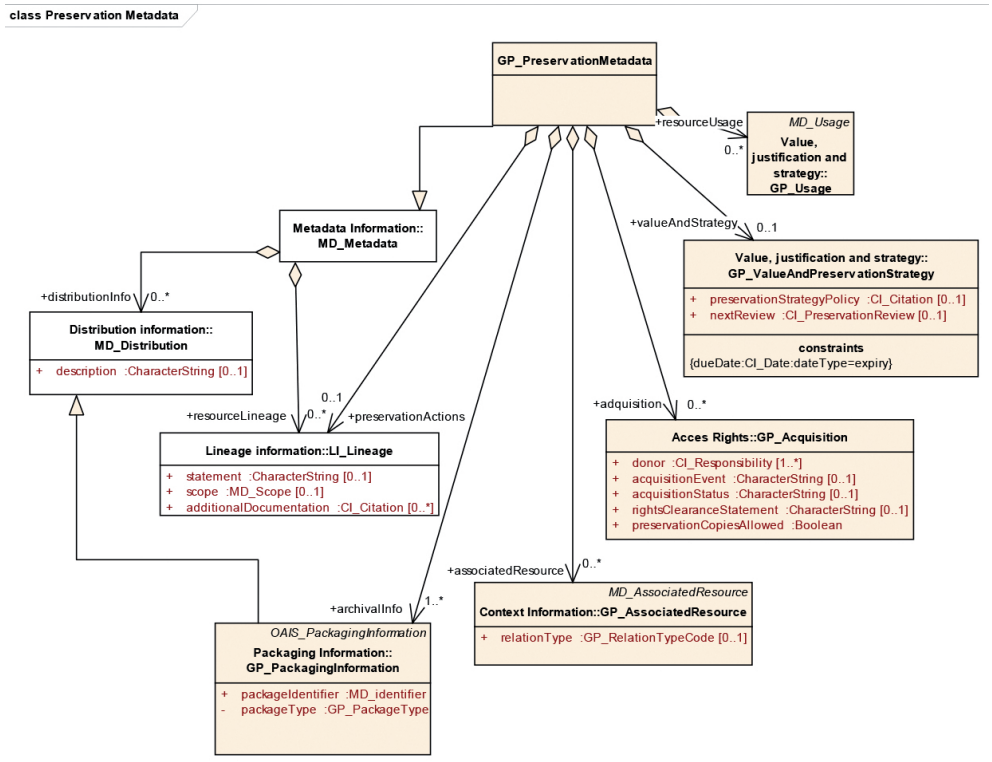

Fig. 2: Top-level classes of the metadata model for preservation (reddish) and the related classes of the ISO 19115-1 (white).

ISO 19115-1 "Metadata – Part 1: Fundamentals" is the metadata standard developed by the ISO/TC 211. The former version (ISO 19115) has been in place for more than a decade and is implemented in numerous environments worldwide. The first revision (ISO 19115-1) is descendent compatible to ISO 19115. It seems natural that the metadata for preservation follow the ISO 19115-1 principles.

ISO 19115-1 defines a comprehensive set of metadata for topics such as distribution, lineage, data formats, spatial and content representation, legal and security constraints, identification, usage, and coordinate reference systems. ISO 19165 will build upon those packages of the ISO 19115-1 metadata model, but define new specific "preservation classes" when the required information cannot be encoded in the ISO 19115-1 model. In addition, for preservation, and within the current ISO 19115-1, it is important to clarify about how to deal with data and metadata identifiers and how to include links to important documentation such as technical specifications, mission concepts, mission definition, data model descriptions. Fig. 2 shows the top-level class of the ISO 19165 model "GP_PreservationMetadata" which itself is a specialization of the MD_Metadata class. This class is shown in the upper left part of the diagram.

The additions to the ISO 19115-1 metadata model are: preservation actions (following the metadata class LI_Lineage), value, use and justification, acquisition, relations to other resources (associated resources), and preservation package information.

Preservation actions are processes that were done by the curators and not by the originally responsible parties of the dataset with the objective of preserving the data, e.g. documenting a media migration. *Value, use and justification* deals with documenting the administrative, legal, evidentiary, research, historically recognized value of the resource and the justification for preserving it, e.g. documenting the legal mandate to preserve the dataset for 10 years for legal purposes. It also includes geospatial services usage statistics, e.g. documenting the number of times the dataset was visualized in a web map service, as another means of justifying the importance of the dataset, the preservation criteria review dates, including the eventual decision of discontinuing the preservation of the resource. *Acquisition* element deals with how, when and with what legal constraints the dataset was given to a preservation body, e.g. including specific licenses agreements and restrictions to package redistribution. *Relations to other resources* reuses the MD_AssociatedResources and includes a PREMIS (PREMIS 2012) relation taxonomy, e.g. the dependency that a geological dataset has to a reference topographical map. *Preservation package information* lists all the parts (files and documents) that together form the AIP, e.g. enumerating all files covering the data values, additional data tables, the metadata, the product specifications, the format specifications, the symbols used in the visualization, and a quicklook in PDF format.

The acronym "GP" is a proposed shortcut that identifies the preservation standard within the ISO/TC 211 family of standards.

4 Next Steps of the Development Process

According to the ISO regulations, the expert's contributions shall be provided on the Working Draft level. This will last at least for the next one year. The following Committee Draft level initiates comments from the Technical Committee 211 "Geographic information / Geomatics". The later stages such as Draft International Standard are reserved for the ISO central secretariat to polish the standard on the editorial level.

The authors, who also chair the project team of the ISO 19165, ask for contributions which refine the proposed model and which eventually allows for the definition of more detailed procedures for a stable and save preservation of geospatial data.

References

CNAATD, 2015: http://cultura.gencat.cat/ca/departament/estructura_i_adreces/organismes/dgpc/temes/arxius_i_gestio_documental/cnaatd/accio_de_la_cnaatd/index.html (5.8.2015).

Engel, H., Engelmeier, S., Grams, G., Gültlinger, M., Häussermann, M., Hermann, C., Hoss, H., Keitel, C., Koch, E., Lang, R., Naumann, K.,

Schurer, H., Spohrer, M., Strietter, O., Witke, T., Wöhrle, M. & Wütherich, T., 2013: Archivierung von Geobasisdaten im Kontext der Gesamtüberlieferung des Vermessungswesens. – Landesamt für Geoinformation und Landentwicklung Baden-Württemberg, Stuttgart.

GDAL, 2015: Supported raster data formats: http://www.gdal.org/formats_list.html, Supported vector data formats: http://www.gdal.org/ogr_formats.html (30.9.2015).

GeoMAPP, 2010: Geospatial Multistate Archive and Preservation Partnership. – http://www.geomapp.net/default.htm (5.8.2015).

Higgins, S., 2008: The DCC Curation Lifecycle Model. – The International Journal of Digital Curation **3** (1): 134–140, http://www.ijdc.net/index.php/ijdc/article/download/69/48 (4.8.2015).

ISO 14721, 2012: Reference Model for an Open Archival Information System (OAIS). – http://public.ccsds.org/publications/archive/650x0m2.pdf (4.8.2015).

Jobst, M. & Gartner, G., 2011: Structural Aspects for the Digital Cartographic Heritage. – Jobst, M. (ed.): Preservation in Digital Cartography – Archiving Aspects, Springer.

Library of Congress, 2010: Appraisal and Selection of Geospatial Data. – 23 p., Library of Congress, Washington D.C., USA.

Library of Congress, 2011: Sustainability of Digital Formats Planning for Library of Congress Collections. – http://www.digitalpreservation.gov/formats/index.shtml (30.9.2015).

LTDP, 2012: Long Term Data Preservation, Earth Observation Preserved Data Set Content, LTDP/PDSC. – 80 p., European Space Agency.

Moe, D. & Longhenry, R., 2013: Metrically Preserving the USGS Aerial Film Archive. – Photogrammetric Engineering & Remote Sensing **2013:** 225–228.

NESDPCS, 2012: NASA Earth Science Data Preservation Content Specification. – Earth Science Data and Information System Project, 423-SPEC-001, 30 p., https://earthdata.nasa.gov/files/423-SPEC-001_NASA ESD_Preservation_Spec_OriginalCh01_0.pdf (30.9.2015).

PREMIS, 2012: Data Dictionary for Preservation Metadata, version 2.2, July 2012 (premis-2-2.pdf). – http://www.loc.gov/standards/premis (5.8.2015).

Ramapriyan, H.K. & Moses, J.F., 2012: NASA Earth Science Data Preservation Content Specification. – 30 p., NASA, 423-SPEC-001, Greenbelt, MD, USA.

Rönsdorf, C., Mason, P., Gerber, U., Bos, M., Shaon, A., Naumann, K., Kirstein, M., Samuelsson, G., Rantala, M., Kvarteig, S. & Stössel, W., 2013: GI+100: Long term preservation of digital Geographic Information – 16 fundamental principles agreed by National Mapping Agencies and Archives. – http://www.eurosdr-ireland.net/archiving/GI+100%20-%2016%20EuroSDR%20Archiving%20Principles_V3%201.pdf (4.8.2015).

Steffen, W., Richardson, K., Rockström, J., Cornell, S.E., Fetzer, I., Bennett, E.M., Biggs, R., Carpenter, S.R., de Vries, W., de Wit, C.A., Folke, C., Gerten, D., Heinke, J., Mace, G.M., Persson, L.M., Ramanathan, V., Reyers, B. & Sörlin, S., 2015: Planetary boundaries: Guiding human development on a changing planet. – Science **347** (6223), 1259855.

Wulder, M.A., Masek, J.G., Cohen, W.B., Loveland, T.R. & Woodcock, C.E., 2012: Opening the archive: How free data has enabled the science and monitoring promise of Landsat. – Remote Sensing of Environment **122:** 2–10.

Addresses of the Authors

Prof. Dr. Wolfgang Kresse, Politechnika Koszalińska, ulica Śniadeckich 2, PL 75-453 Koszalin, Tel.: +48-94-34-86-728, e-mail: wolfgang.kresse@tu.koszalin.pl

Dr. Joan Masó Pau, CREAF, Fac. Ciencies, Edifici C, Universitat Autònoma de Barcelona, Tel.: +34-93-581-1771, Fax: +34-93-581-4151, e-mail: joan.maso@uab.cat

Manuskript eingereicht: August 2015
Angenommen: Oktober 2015

Berichte von Veranstaltungen

14. Internationales 3D-Forum Lindau, 5. – 6. Mai 2015

Das 14. Internationale 3D-Forum Lindau fand am 5. und 6. Mai 2015 im Kongresszentrum Inselhalle Lindau statt und erreichte mit 220 Teilnehmern aus 8 Ländern einen neuen Höchststand. An der tagungsbegleitenden Ausstellung nahmen 25 Firmen aus 5 Ländern teil, vornehmlich aus den Anwendungsbereichen 3D-Visualisierung, GIS, Mobile Mapping, LIDAR und Photogrammetrie.

Die Veranstalter Dipl.-Ing. Claus Bihl (Stadt Lindau) und Dr.-Ing. Achim Hellmeier (Ingenieurbüro Real.IT, Aalen) hatten unter den Schwerpunktthemen *Vom 2D-GIS zum 3D-WebGIS, 3D-Stadtmodelle in Architektur und Stadtplanung, Internetvisualisierung und 3D-Apps und Augmented Reality in der Geoinformation* wieder ein sehr aktuelles Programm erstellt mit Referenten aus Wirtschaft, Wissenschaft und Verwaltung. Erstmals wurde auch in zwei Beiträgen näher auf Building Information Modeling (BIM) eingegangen.

Neben den bisherigen Partnern der Veranstaltung, der Gesellschaft für Geodäsie, Geoinformation und Landmanagement (DVW), der Deutsche Gesellschaft für Photogrammetrie, Fernerkundung und Geoinformation (DGPF), dem Virtual Dimension Center (VDC) Stuttgart/Fellbach kam in diesem Jahr ein neuer Partner, nämlich der DDGI (Deutscher Dachverband für Geoinformation e.V.), hinzu. Hauptsponsor der Veranstaltung war die Firma Esri Deutschland GmbH.

Wie in den Vorjahren wurde die Veranstaltung in einen Vortragsteil am ersten Tag und in Vertiefungsthemen und Workshops am zweiten Tag aufgeteilt.

Gerhard Ecker, Oberbürgermeister der Stadt Lindau, eröffnete das 14. Internationale 3D-Forum Lindau. Er hob in seiner Begrüßungsrede hervor, dass die Stadt Lindau mitten in der Planungsphase des Großprojektes „Neues Kongresszentrum Inselhalle“ steckt und dass dabei das 3D-Stadtmodell von Lindau vor allem für die Bürgerbeteiligung eine wichtige Rolle spiele. Die abschließende Planung wurde dabei in das 3D-Stadtmodell fotorealistisch integriert.

Nach der Eröffnung durch den Oberbürgermeister überbrachte Udo Stichling, Präsident des DDGI ein kurzes Grußwort des DDGI als neuen Partner des 3D-Forums. Anschließend übernahm Achim Hellmeier die Moderation der Veranstaltung in bekannt temperamentvollem Stil. Der erste Vortragende, Gerd Buziek, Vizepräsident des DDGI, ging in sei-

Abb. 1: Veranstaltungsort Inselhalle Lindau.

DOI: 10.1127/pfg/2015/0281 1432-8364/15/0281 $ 6.25

nem Vortrag *3D-WebGIS im Spannungsfeld von Smart Cities und Social Media* auf die gesellschaftlichen und technologischen Treiber neuer GIS-Entwicklungen ein und zeigte eine Reihe interessanter Beispiele dazu. Im nächsten Beitrag zeigte Marc Orban von der Stadt Luxemburg an sehr instruktiven Beispielen, wie das 3D-Stadtmodell in Luxemburg genutzt wird. Orban gab auch einen Einblick in die organisatorische Struktur der Stadtverwaltung und wie darin das Thema 3D eingebunden ist.

Den zweiten Vortragsblock eröffnete Max Lang vom Amt für Ländliche Entwicklung Schwaben. In seiner Präsentation *Virtuelle Modelle für Bürgerbeteiligungen im Rahmen von Dorfsanierungen* kam deutlich heraus, wie wichtig moderne Werkzeuge im Planungsprozess vor allem auch im Hinblick auf die Akzeptanz von Planungen durch die Bürger sind. Der letzte Vortrag im Vormittagsprogramm kam vom Planungsbüro HWP Planungsgesellschaft mbH Stuttgart. Dereje Alemu stellte unter dem Titel *3D-Stadtmodelle aus Sicht des Architekten und Stadtplaners* Projekte vor, in denen Teile aus 3D-Stadtmodellen im Planungsprozess genutzt werden. Für die zahlreichen Teilnehmer aus der „Geobranche“ war es sehr interessant, wie der Architekt und Stadtplaner 3D-Geobasisdaten beurteilt. Alemu machte auch deutlich, dass 3D-Stadtmodelle im Hinblick auf BIM an Bedeutung gewinnen werden.

Um den Tagungsteilnehmern ein gezieltes Zugehen auf die ausstellenden Firmen zu erleichtern, stellten die Veranstalter vor der Mittagspause die beteiligten Firmen in Kurzporträts vor.

Das Nachmittagsprogramm eröffnete Jürgen Döllner vom Hasso-Plattner-Institut in Potsdam. Unter der Überschrift *Internet und App als effektive Medien für 3D-Stadtinformation* zeigte Döllner sehr anschaulich an verschiedenen Beispielen die Möglichkeiten, Grenzen und Entwicklungstrends dieser Technologien auf. Danach berichtete Henri Eisenbeiss von der Stadt Winterthur (Schweiz) über *UAVs im kommunalen Bereich – Anwendungen und Erfahrungen*. Hervorzuheben sind hier unter anderem technische und aufwandsmäßige Vergleiche von UAVs mit anderen Messmethoden.

Der finnische Architekt Anssi Savisalo von FCG (Finish Consulting Group) stellte in seinem Beitrag die *Moderne Stadtplanung in 3D – Aktuelle Lage in Finnland* vor. Neben den städteplanerischen Aspekten waren auch die Ausführungen von Savisalo zum Thema Schnittstellen und BIM sehr aufschlussreich. Er sieht als zukünftige nationale Geobasis in Finnland die Kombination von klassischen Geobasisdaten, 3D-Stadtmodellen und BIM-Daten. Im letzten Vortrag des ersten Veranstaltungstages referierte dann Martin Wessels vom Institut für Seenforschung der LUBW (Landesanstalt für Umwelt, Messun-

Abb. 2: Firmenpräsentationen in Foyer der Inselhalle.

gen und Naturschutz Baden-Württemberg) über *Das Projekt Tiefenschärfe – Der Bodensee präzise in 3D*. Dieser Vortrag war ein schöner Abschluss, da er neben anspruchsvollen messtechnischen Verfahren und Lösungen auch äußerst interessante Fakten über das 254 m tiefe Schwäbische Meer zu Tage brachte.

Mit einem geselligen Beisammensein auf der Insel Lindau im historischen Gasthaus Sünfzen klang der erste Veranstaltungstag aus. Dieser Abend ist traditionell fester Bestandteil des 3D-Forums Lindau und führte bei guter Stimmung wieder einmal zu einem angeregten Gedankenaustausch zwischen den Teilnehmern.

Der zweite Veranstaltungstag begann mit drei Vertiefungsthemen am Vormittag. Am Nachmittag folgten dann mehrere Workshops. Das erste Vertiefungsthema *Augmented Reality in der 3D-Geoinformation* wurde von Volker Coors von der Hochschule für Technik Stuttgart präsentiert. Mit den Unterpunkten Technische Grundlagen, Anwendungen/Beispiele und dem neuen OGC-Standard der ARML (Augmented Reality Markup Language) erhielten die Teilnehmer einen sehr guten Überblick zu Augmented Reality. Im zweiten Vertiefungsthema referierte Thomas Kersten von der HafenCity Universität Hamburg über *Die Punktwolke als wesentliche Grundlage für 3D-Gebäudemodelle*. Er zeigte sehr anschaulich den Workflow von der Datenerfassung über die Modellierung hin zur Visualisierung auf und hinterlegte das Ganze mit sehr eindrucksvollen Beispielen. Der letzte Vortrag dieses Blocks trug die Überschrift 3D-Druck weiter im Aufwind. Er wurde von Karl-Heinz Häfele vom Institut für Angewandte Informatik des KIT Karlsruhe gehalten. Neben den Grundlagen, dem Modellaufbau und den verschiedenen Verfahren gab Häfele an Hand von Beispielen wichtige eigene Erfahrung beim 3D-Druck weiter.

Nach Abschluss des eigentlichen Vortragsprogramms folgten dann am Nachmittag die Workshops. Neben fünf Firmenworkshops fand zum fünften Mal der CityGML Workshop mit Experten aus der SIG3D und der Standard Working Group des OGC statt. Hier standen die stadtweite Energiebedarfsabschätzung und die Energy ADE (Application Domain Extension) im Vordergrund. Neben den technischen Neuerungen und Informationen wurde in diesem Workshop sehr angeregt und konstruktiv diskutiert. Firmenworkshops wurden von Esri, Lothhamer & Zirn Consulting, M.O.S.S. Computer Graphik Systeme, VirtualCitySystems und UVM Systems abgehalten. Die Firmenworkshops fanden durchweg starkes Interesse und waren gut besucht.

Die Workshops bildeten damit auch den Abschluss der Veranstaltung, die gegen 17 Uhr zu Ende ging. Zusammenfassend lässt sich festhalten, dass das 14. Internationale 3D-Forum Lindau nicht nur wegen der hohen Teilnehmer- und Ausstellerzahl als voller Erfolg gewertet werden kann, sondern vor allem auch wegen der interessanten Vorträge und Firmenpräsentationen. Den beiden Veranstaltern, Claus Bihl und Achim Hellmeier ist es erneut gelungen, einen spannenden Mix aus praxisorientierten und innovativen Beiträgen zu gestalten. Die stark gewachsene Teilnehmerzahl und die ebenso deutlich zugenommene Beteiligung an der Firmenausstellung haben gezeigt, dass das Thema der 3D-Modellierung im Geobereich längst den Status eines speziellen Forschungsbereichs verlassen hat, wirtschaftlich sehr interessant geworden ist und auch in der Verwaltungspraxis Einzug hält.

Das nächste Internationale 3D-Forum Lindau findet am 10. und 11. Mai 2016 statt (www.3d-forum.li).

Peter Ladstätter, Erding

Jahrestagung AK Fernerkundung „Daten – Informationen – Entscheidungen“ 24. – 25.9.2015, Bonn

Unter dem Motto „Daten – Informationen – Entscheidungen“ fand vom 24. bis zum 25. September 2015 die 4. gemeinsame Jahrestagung des AK Fernerkundung der Deutschen Gesellschaft für Geographie (DGfG) e.V. und des AK Auswertung von Fernerkundungsdaten der Deutschen Gesellschaft für Photogrammetrie, Fernerkundung und Geoinformation (DGPF) e.V. im Geozentrum der Rheinischen Friedrich-Wilhelms-Universität Bonn statt. Organisiert wurde die Tagung von

Frank Thonfeld, Olena Dubovyk und Gunter Menz, der Arbeitsgruppe Fernerkundung, Geographisches Institut der Universität Bonn sowie Zentrum für Fernerkundung der Landoberfläche der Universität Bonn.

Etwa 40 Teilnehmende aus Deutschland und Österreich sowie ca. 20 Mitarbeiter und Mitarbeiterinnen sowie Studierende der Universität Bonn nahmen an der zweitägigen Veranstaltung teil. Das breit gefächerte Programm aus Keynote- und Fachvorträgen, interaktiven „hands-on workshops“ und einer Postersession wurde äußerst positiv aufgenommen. Die drei Keynote-Vorträge behandelten aktuelle Themenfelder der angewandten Fernerkundung und den Status laufender und zukünftiger europäischer Erdbeobachtungsmissionen. Vanessa Keuck vom Deutschen Zentrum für Luft- und Raumfahrt (DLR) stellte das Copernicus-Programm vor und erläuterte, wie die Wissenschaft darin eingebunden ist. Sabine Chabrillat vom Geoforschungszentrum Potsdam (GFZ) referierte über den aktuellen Stand der EnMap-Mission, einer deutschen Hyperspektralsatellitenmission, deren Daten ab 2018 erhältlich sein sollen. Vielbeachtet war auch die Keynote von Joachim Post (UN-SPIDER), der die Bedeutung der Erdbeobachtung für das Krisenmanagement hervorhob.

Im Rahmen der beiden angegliederten Workshops wurden aktuelle Themenfelder der Fernerkundung mit modernster Software praktisch bearbeitet. Das Ziel, vor allem junge Wissenschaftler und Wissenschaftlerinnen zu Vorträgen zu motivieren und ein Forum zur Präsentation und Diskussion ihrer Studien und zum Austausch zu bieten, konnte aus Sicht der Organisatoren erreicht werden.

Während der abschließenden Diskussion wurden Anregungen für das zukünftige Format der Veranstaltung eingeholt. Insbesondere die Vielfältigkeit und der Raum für Gespräche wurden als positiv hervorgehoben. Die Veranstalter, das Geographische Institut der Universität Bonn (AG Fernerkundung) und dem Zentrum für Fernerkundung der Landoberfläche (ZFL), bedanken sich bei allen Teilnehmer/Innen für die hochwertigen Beiträge und den regen Austausch sowie bei den Sponsoren DLR, Harris/Exelisvis und Geosystems für die Unterstützung.

Das vollständige Programm kann unter https://akfe.geographie.ruhr-uni-bochum.de/images/20150922_AK_Programm_v09.pdf eingesehen werden.

Gunter Menz, Bonn

Hochschulnachrichten

First Joint PhD Colloquium on Geoinformatics of DGK and DGPF

From February 16 to 17, 2015, the first joint PhD colloquium of the DGPF working group on geoinformatics and the DGK section for geoinformatics was held at the University of Osnabrück. The colloquium aimed at strengthening algorithmic and methodological competencies, stipulating exchange between PhD candidates, and enhancing presentation and discussion skills. The program was thus set up to include presentations by PhD candidates, intensive discussions, which were chaired by the young scientists, as well as focused discussions in small working groups. An overview of bibliometrics was given by Ralf Bill, University of Rostock. The PhD colloquium was followed by a tutorial on mathematical programming, which was held by Jan-Henrik Haunert, University of Osnabrück. Lars Bernard, University of Dresden, completed the organization team.

As the result of an abstract-based review process, seven PhD students had been invited to give an in-depth (full) presentation of their work. Those PhD students presented their work in three sessions, which were dedicated to automated cartography, augmented reality, and algorithmic foundations of geoinformatics and photogrammetry. Participants without a full presentation had the opportunity to introduce themselves with a short talk.

Considering the very positive feedback from the participants, the colloquium, in the chosen format, was a full success. The Bohnenkamphaus in the botanical garden of the University of Osnabrück turned out to be the ideal location for the event, not least because it allowed for a relaxing walk to the historical centre of Osnabrück, where the first day of the colloquium ended with conversations over pizzas and drinks.

The geoinformatics groups of DGK and DGPF aim to establish the PhD colloquium as an annual event. For 2016, the colloquium is planned to be held at the University of Bonn. Invitations will be forwarded via the subscription lists of DGPF and DGK.

Karlsruher Institut für Technologie

Habilitation von Dr.-Ing. Boris Jutzi

Herr Dr.-Ing. Boris Jutzi habilitierte am 22.7.2015 an der Fakultät für Bauingenieur-, Geo- und Umweltwissenschaften des Karlsruher Instituts für Technologie (KIT) mit der Arbeit *Methoden für neue aktive optische Sensoren zur automatischen Szenencharakterisierung in der Photogrammetrie und Fernerkundung.*

1. Referent: Prof. Dr.-Ing. habil. Stefan Hinz, KIT,
2. Referent: Prof. Dr.-Ing. habil. Richard Bamler, TU München und DLR
3. Referent. Prof. Dr.-Ing. habil. Hans-Gerd Maas, TU Dresden.

In Photogrammetrie und Fernerkundung finden seit einigen Jahren neue, teils prototypisch experimentelle, teils aber auch schon operationelle Sensorsysteme Eingang. Deren Entwicklungszweck ist nicht mehr einzig die Schaffung einer 2D- oder 3D-Datengrundlage für die Vermessung, Extraktion oder Charakterisierung natürlicher oder anthropogener Objekte. Vielmehr begründen sich die Entwicklungslinien und Spezifikationen häufig mit den Erfordernissen anderer Märkte. Typisches Beispiel hierfür ist die neue Generation an Spielekonsolen, deren 3D-Messdaten und beispielweise auch die nachfolgende Posenerkennung auf bekannten photogrammetrischen Prinzipien beruhen, deren entwicklungstechnische Vorgaben jedoch mehr dem Ziel einer weltweiten Positionierung in einem „wohnzimmertauglichen“ Massenmarkt und nicht einer Verwendung im Kontext von photogrammetrischen oder fernerkundlichen Aufgabenstellungen folgen. Im Umkehrschluss motivieren derartige kostengünstige Sensoren jedoch eine vertiefte wissenschaftliche Aus-

einandersetzung und die Entwicklung neuer Modelle und Methoden für die Auswertung der Daten. Die hierdurch gewonnenen Erkenntnisse eröffnen weitere Horizonte, um einerseits bisherige Kernaufgaben in Photogrammetrie und Fernerkundung deutlich günstiger und flexibler zu bearbeiten. Andererseits werden dadurch auch völlig neue Anwendungsfelder erschlossen, die mit der klassischen Sensorik nicht in Reichweite wären.

Besonders interessant in diesem Zusammenhang sind die so genannten „aktiven Sensoren", deren Datenerfassung auf einem vom Sensor ausgesandten Messsignal beruht. Im Gegensatz zu herkömmlichen Kameras sind diese Sensoren nicht von einer externen Beleuchtungsquelle abhängig und erfordern für eine 3D-Rekonstruktion der aufgezeichneten Oberflächen in der Regel auch keine Textur. Limitierungen – je nach Sensor unterschiedlich stark ausgeprägt – herrschen jedoch in Aspekten wie beispielsweise geometrischer und radiometrischer Genauigkeit, Reichweite und Einsatz im Außenraum bzw. bei Sonnenlicht.

An diesen Punkten setzt die Habilitationsarbeit an. Mit Anschluss an die in Photogrammetrie und Fernerkundung seit gut 15 Jahren etablierte Technik des (Präzisions-) Laserscannings konzeptioniert und entwickelt die Habilitationsarbeit fortgeschrittene Auswerteverfahren für Messdaten der neuen aktiven Sensoren, deren Gesamtkonzeption von der Modellierung und Detektion des rohen Messsignals bis hin zur Charakterisierung ganzer Szenen reicht. Die tiefgreifende Untersuchung und Modellierung der Sensor- und Dateneigenschaften des jeweiligen Sensors sind dabei integraler Bestandteil der Arbeit.

Die kumulativ gestaltete Habilitationsschrift gliedert sich in zwei Teile. Der erste Teil umfasst vier Kapitel, wobei die ersten drei Kapitel auf ca. 50 Seiten eine Zusammenfassung über die Konzeption, die grundlegenden Methoden sowie die Erkenntnisse und Anschlussmöglichkeiten der Arbeit geben. In diesen Kapiteln wird aufbauend auf einer Taxonomie der aktiven Sensorik ein Gesamtkonzept zur automatischen Szenencharakterisierung vorgestellt und anhand verschiedener aktiver Sensoren mit den entsprechenden neuartigen Methoden sowie Anwendungsbeispielen und Evaluierungen untermauert. Kapitel 4 erläutert die Abbildung der eingebrachten Publikationen auf die Struktur der Arbeit. Der zweite Teil der Habilitationsschrift umfasst 22 Schlüsselpublikationen und etwa ebenso viele weiterführende Publikationen, die das wissenschaftliche Rückgrat der Arbeit darstellen.

Dissertation von Simon Schuffert

Herr Dipl.-Ing. Simon Schuffert wurde am 13.7.2015 an der Fakultät für Bauingenieur-, Geo- und Umweltwissenschaften des Karlsruher Instituts für Technologie (KIT) mit der Arbeit *Punktkorrespondenzen in Bildpaaren aus projektiven und radiometrischen Invarianzen* zum Dr.-Ing. promoviert.

1. Referent: Prof. Dr.-Ing. habil. Stefan Hinz, KIT,
2. Referent: apl. Prof. Dr. techn. Franz Rottensteiner, Universität Hannover.

Kurzfassung:
Eine fundamentale Voraussetzung für sehr viele Anwendungen in der Photogrammetrie und in der Computer Vision ist es, identische Punkte eines abgebildeten Objektes in zwei sich überlappenden Bildern zu finden. Diese Fähigkeit der automatischen Zuordnung gleicher Objekte ist zwar für ähnliche Ansichten von Objekten gelöst, jedoch nicht für starke Abweichungen von verfahrensinhärenten Annahmen.

Zum Auffinden von Punktkorrespondenzen ist das Identifizieren homologer Objektpunkte in unterschiedlichen Bildern notwendig. Die Zuordnungen von Pixeln im ersten Bild zu ihren Entsprechungen im zweiten Bild, geschehen über gleiche Merkmale. Dafür werden bisher meistens lokale Merkmale in beiden Bildern beschrieben, die dann miteinander verglichen werden. Aktuelle Featuredeskriptoren wie Harris, Harris-Affine, SIFT, SURF, FAST, MSER, ORB, BRISK oder ASIFT beschreiben punktbezogene oder blobbezogene Merkmale, die für einen automatischen Algorithmus gut zuzuordnen sind. Diese Merkmalsdeskriptoren beschreiben die kleinräumige Textur um ein Pixel und erlauben eine robuste Zuordnung bei geringen Änderungen des Blickwinkels gegenüber dem Objekt,

wenn die Aufnahmezeitpunkte sehr nah beieinander liegen und auch wenn für beide Bilder der gleiche Sensortyp benutzt wurde. Bei stark unterschiedlichen Blickpunkten auf ein dreidimensionales Objekt können diese Featuredeskriptoren hingegen keine korrekten Ergebnisse liefern. Deutliche Änderungen in der Radiometrie des Bildes aufgrund unterschiedlicher Beleuchtungen oder auch veränderte Schattenverläufe aufgrund unterschiedlicher Tageszeitpunkte verhindern erfolgreiche Punktzuordnungen. Auch der Ansatz des *Bag of visual words*, der eine allgemeinere Bildbeschreibung liefert, ist aufgrund der verwendeten Algorithmen lediglich invariant gegenüber affinen Transformationen.

Der zentrale Ansatz der vorliegenden Arbeit zur Lösung dieser Herausforderungen ist folgender: Beide Bilder enthalten zweidimensionale Abbildungen von identischen dreidimensionalen Objekten, die mit einer Zentralprojektion auf die Bildebene abgebildet wurden. Beiden Bildern gemeinsam ist somit, dass Ebenen eines Objektes mit einer projektiven Transformation abgebildet wurden. Zum Auffinden von identischen Punkten werden gleiche Eigenschaften in beiden Bildern gesucht, die sich durch eine projektive Transformation nicht verändern und somit projektiv invariant sind. Beide Bilder werden daher nur mit Hilfe von Eigenschaften beschrieben, die projektiv invariant sind. Anschließend werden diese Bildbeschreibungen miteinander verglichen und die damit verbundenen identischen Punkte einander zugeordnet. Diese projektiv invarianten Eigenschaften sind im Einzelnen: Das Doppelverhältnis von vier Punkten auf einer projektiven Geraden, die zwei Invarianten I_1 und I_2 von fünf Punkten auf einer projektiven Ebene, die Konnektivität von Punkten, die Inzidenzen von Punkten sowie die Beibehaltung gerader Linien. Um unabhängig von der Variabilität der Radiometrie zu sein, werden die Punktzuordnungen ausschließlich anhand von Gradientenamplituden beschrieben.

Die Verwendung einzelner projektiv invarianter Eigenschaften zum Bestätigen identischer Bildpunkte ist grundsätzlich nicht neu. Die Neuheit und das wesentliche Alleinstellungsmerkmal der Arbeit bestehen darin, dass die Beschreibung eines Bildes mittels mehrerer kombinierter projektiv invarianter Eigenschaften abgegeben wird. Diese Kombination führt zu völlig neuen Möglichkeiten der Korrespondenzsuche. Ein weiterer Vorteil dieses Lösungsansatzes ist, dass dieser auch auf Bilder anwendbar ist, die mit einfacheren Transformationen abgebildet wurden, da die projektiv invarianten Eigenschaften auch Invarianz gegenüber einfacheren Transformationen inkludieren wie beispielsweise eine Ähnlichkeitstransformation oder eine affine Abbildung. Eine Lösung des Zuordnungsproblems für projektive Abbildungen löst daher auch das Zuordnungsproblem bei untergeordneten Transformationen.

Die Ergebnisse der Arbeit und die durchgeführten Experimente zeigen, dass, unter der Voraussetzung, dass eine Szene partiell aus Ebenen zusammengesetzt ist, mittels kombinierter projektiv invarianter Merkmale auch unter solchen Bedingungen Punktzuordnungen für eine photogrammetrische Weiterverarbeitung gefunden werden können, wo bisherige Verfahren keine zuverlässigen Ergebnisse mehr liefern, so z.B. bei Blickwinkeländerungen weit über 45 Grad. Des Weiteren zeigt die Arbeit, dass die bei projektivinvarianten Verfahren häufig kritisierten hohen Rechenzeiten durch eine geschickte sequentielle und teils iterative Kombination der projektiv invarianten Merkmale bei der Korrespondenzsuche stark eingeschränkt werden können.

Die Dissertation ist im Verzeichnis der Bibliothek des Karlsruher Instituts für Technologie online verfügbar.

HafenCity Universität Hamburg

Dissertation von Christoph Kinkeldey

Herr Dipl.-Ing. Christoph Kinkeldey wurde am 19.1.2015 im Fachbereich Geomatik an der HafenCity Universität Hamburg mit der Arbeit *Incorporating unvertainty information into exploratory land cover change analysis: a geovisual analytics approach* zum Dr.-Ing. promoviert.

1. Referent: Prof. Dr. Jochen Schiewe, HafenCity Universität Hamburg,
2. Referent: Prof. Dr. Alan MacEachren, Pennsylvania State University, USA,

3. Referent: Prof. Dr. Alexander Klippel, Pennsylvania State University, USA.

Kurzfassung:
In den vergangenen Jahrzehnten wurde intensiv Forschung betrieben, um Unsicherheiten in Geodaten zu beschreiben, zu quantifizieren und nutzbar zu machen. Praktisch einsetzbare Modelle und Methoden für diesen Zweck sind jedoch selten, und die Effekte durch Kommunikation von Informationen zu Unsicherheiten bei räumlichen Analysen sind noch nicht ausreichend erforscht. Die Dissertation widmet sich diesen Herausforderungen und konzentriert sich dabei auf Veränderungsanalysen von Landbedeckung auf Basis von Fernerkundungsdaten, bei denen Unsicherheiten eine wichtige Rolle spielen.

Das in der Dissertation beschriebene Vorhaben zielt darauf ab, ein Konzept nach dem „Geovisual Analytics" (GVA)-Ansatz zu entwickeln, um Unsicherheiten bei Veränderungsanalysen zu berücksichtigen. Dieser Ansatz ermöglicht Arbeitsabläufe, die automatische Algorithmen mit interaktiven visuellen Schnittstellen vereinen, um die Stärken von maschineller Berechnung mit denen der menschlichen Interpretation zu verbinden. Die zentrale Frage dieser Arbeit war, ob Nutzer bei Verwendung eines GVA-Tools von Unsicherheitsinformationen profitieren. Die Kernfrage ist, ob diese beim Aufstellen von Hypothesen und beim Erlangen von Erkenntnissen während Veränderungsanalysen helfen.

Es wurde ein Konzept für die Einbeziehung von Unsicherheiten in Veränderungsanalysen der Landbedeckung entwickelt. Dabei bestanden die wichtigsten Schritte in der Definition eines Unsicherheitsmaßes für Landbedeckungsveränderungen, der Auswahl, Implementierung und Evaluierung einer Technik zur Darstellung von Unsicherheiten in Veränderungskarten („Noise Annotation Lines"), sowie der Erstellung einer Kategorisierung von Tasks in explorativen Veränderungsanalysen. Eine Fallstudie mit realen Veränderungsdaten zur Landbedeckung demonstrierte die Anwendbarkeit des Konzepts. Eine systematische Übersichtsarbeit von Nutzerstudien zur Visualisierung von Unsicherheiten diente als Basis für die Auswahl einer geeigneten Visualisierungsmethode. Ergebnisse der Studien wurden zusammengefasst, „Lessons Learned" formuliert, sowie Empfehlungen für zukünftige Studien gegeben. Ein neuartiges Modell für die Kategorisierung von Visualisierungsmethoden („Uncertainty Viusalization Cube, UVis³") wurde als Basis für eine systematischere Auswahl und Evaluation von Methoden zur Unsicherheitsvisualisierung in der Zukunft vorgeschlagen. Als Machbarkeitsnachweis sowie als Grundlage für eine Expertenstudie, mit welcher die Praktikabilität des hier entwickelten Konzepts überprüft wurde, konnte ein Software-Prototyp für die Änderungsanalyse mit Unsicherheiten („ICchange") entwickelt werden. Dessen Entwicklung umfasste auch eine Verbal Protocol Analysis (VPA)-Studie, um die Gebrauchstauglichkeit des Prototyps zu überprüfen.

In einer anschließenden Studie mit drei Gruppen von Experten, die Landbedeckungsanalysen in der Praxis durchführen, wurde die Praktikabilität des entwickelten Konzepts überprüft. In semi-strukturierten Gruppeninterviews wurde der Software-Prototyp eingesetzt, um verschiedene den Experten bereits vertraute Änderungsszenarien zu demonstrieren, angereichert mit Informationen über Unsicherheiten in den Ergebnissen. Generell sahen die Teilnehmer das Konzept für die Unterstützung von Änderungsanalysen als nützlich an, und eine Vielzahl potenzieller Anwendungen wurde diskutiert. Barrieren für den Einsatz in der Praxis wurden ebenfalls angesprochen, wie beispielweise die fehlende Unterstützung durch gängige GIS-Software sowie Vorbehalte, Unsicherheitsinformationen an die Nutzer der Daten zu weiterzugeben. Die Meinungen der Experten zum „ICChange"-Software-Prototyp und zur „Noise Annotation Lines"-Methode waren vorwiegend positiv. Aus den Ergebnissen der Studie und aus Erfahrungen während der Entwicklung des Prototyps wurden Empfehlungen für die Umsetzung des Konzepts in die Praxis gegeben sowie zukünftige Forschungsfragen formuliert.

Preisträger des Karl-Kraus-Nachwuchsförderpreises

Mit dem Karl-Kraus-Nachwuchsförderpreis sollen herausragende Diplom-, Bachelor- und Master-Arbeiten gewürdigt werden. Der Preis wird seit 2007 gemeinsam von der DGPF, der SGPF (Schweiz) und der OVG (Österreich) verliehen und erinnert an Karl Kraus, den bekannten Hochschullehrer und Lehrbuchautor der TU Wien, der 2006 verstarb.

1. Preis: Corinne Stucker, Zürich, Schweiz

Klassifizierung von Vegetation in einer Laserscan-Punktwolke

Motivation und Zielsetzung

Terrestrisches Laserscanning gewinnt im Bereich der Holz- und Forstwirtschaft zunehmend an Bedeutung. Im Gegensatz zu herkömmlichen Waldinventurverfahren, die durch einen hohen Arbeits- und Zeitaufwand gekennzeichnet sind und nur stichprobenartig Informationen liefern, erlaubt terrestrisches Laserscanning eine zeitnahe und präzise Erfassung von Waldbeständen. Aus Laserscan-Punktwolken können forstinventur-relevante Geometrieparameter bestimmt und die eigentlichen Zielgrössen wie Holzvorrat oder Biomasse abgeleitet werden.

Unabhängig vom Anwendungsbereich stellt die semantische Interpretation von Punktwolken einen wesentlichen Schritt für deren Auswertung dar. In Anbetracht der großen Datenmengen und der ungewohnten und inhomogenen 3D-Verteilung der Scanpunkte ist eine manuelle Klassifizierung von Punktwolken zu vertretbaren Kosten jedoch kaum mehr möglich. Vielmehr wird eine möglichst vollständig automatisierte Punktwolkenanalyse und -verarbeitung angestrebt. Im Rahmen dieser Bachelor-Arbeit wurde deshalb ein Klassifikationsalgorithmus für die automatische Attributierung von 3D-Punktwolken statischer, terrestrischer Laserscans erarbeitet, wobei der Fokus auf die Differenzierung zwischen Baumkrone, Baumstamm und Boden gelegt wurde.

Methodik

Als Klassifizierungsansatz wird zum einen Naïve Bayes als klassisches generatives Verfahren und zum anderen Random Forests als modernes diskriminatives Verfahren getestet. Für beide Ansätze erfolgt die Klassifizierung auf Grundlage von Merkmalen, welche die räumliche Verteilung und Ausrichtung der Punkte innerhalb der Nachbarschaft eines LiDAR Punktes charakterisieren bzw. die räumliche Beziehung zwischen einem Punkt und

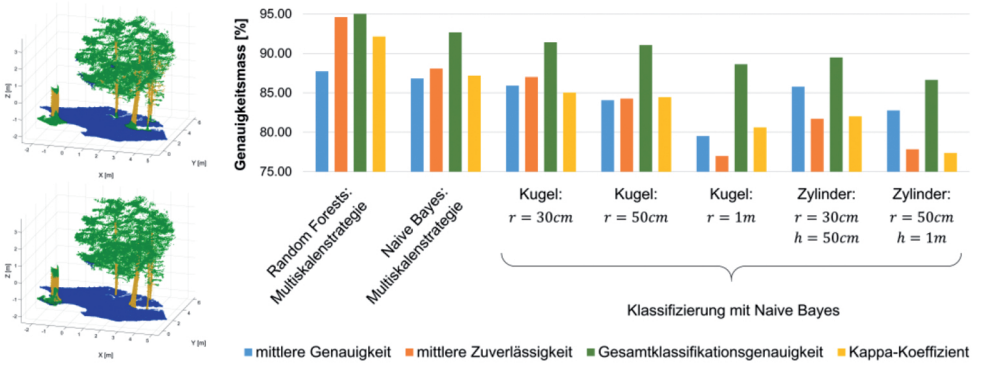

Abb. 1: Klassifizierungsergebnis mit *Naïve Bayes* (links oben) bzw. *Random Forests* (links unten) durch Anwendung der Multiskalenstrategie (blau: Boden, braun: Baumstamm, grün: Baumkrone), aus der Konfusionsmatrix abgeleitete Genauigkeitsmaße der Klassifizierung in Abhängigkeit von der Klassifizierungsmethode und der Nachbarschaftsdefinition (rechts).

seinen benachbarten Punkten erfassen. Die insgesamt 14 implementierten Merkmale beruhen vorwiegend auf Chehata et al. (2009) und lassen sich in nachfolgende drei Typen unterteilen: Merkmale basierend auf der Höhe von LiDAR-Punkten, Merkmale basierend auf den Eigenwerten der lokalen Punktnachbarschaft sowie Merkmale basierend auf der bestangepassten Ebene der lokalen Punktnachbarschaft. In Anlehnung an Brodu & Lague (2012) wird die Merkmalsextraktion sowohl für die kugelförmige als auch für die zylindrische Punktnachbarschaft auf mehreren Maßstabsstufen vorgenommen, um der Problematik der variablen Punktwolkendichte gerecht zu werden (Multiskalenstrategie: Kugel- und Zylinderradius **r** von 30 cm, 50 cm bzw. 1 m sowie halbe Zylinderhöhe **h** von 50 cm bzw. 1 m).

Ergebnisse

Die adaptierten Merkmale wurden ursprünglich für die Klassifizierung von Punktwolken aus Airborne Daten entwickelt. Die Evaluierung zeigt, dass diese Merkmale auch für die Klassifizierung von terrestrischen Punktwolken zweckmässig sind und sich im Speziellen eignen, um Vegetation in Punktwolken zu differenzieren (Abb. 1, links).

Die Qualität der Klassifizierung ist maßgeblich von der Art und Dimension der zugrundeliegenden Punktnachbarschaft abhängig (Abb. 1, rechts). Die höchsten Genauigkeitsmaße werden sowohl bei der Klassifizierung mit Naïve Bayes als auch mit Random Forests durch Anwendung der Multiskalenstrategie erzielt. Verbesserungspotenzial des Klassifikationsalgorithmus ist einerseits durch die automatische Bestimmung von optimalen Nachbarschaftsgrößen (Weinmann et al. 2014) oder durch die Einführung von nachbarschaftsgrößen-unabhängigen Merkmalen (Blomley et al. 2014) gegeben.

Referenzen

Brodu, N. & Lague, D., 2012: 3D terrestrial lidar data classification of complex natural scenes using a multi-scale dimensionality criterion: Applications in geomorphology. – ISPRS Journal of Photogrammetry and Remote Sensing **68:** 121–134.

Blomley, R., Weinmann, M., Leitloff, J. & Jutzi, B., 2014: Shape distribution features for point cloud analysis – a geometric histogram approach on multiple scales. – ISPRS Annals of the Photogrammetry, Remote Sensing and Spatial Information Sciences **II-3:** 9–16.

Chehata, N., Guo, L. & Mallet, C., 2009: Airborne lidar feature selection for urban classification using random forests. – International Archives of the Photogrammetry, Remote Sensing and Spatial Information Sciences **39** (3/W8): 207–212.

Weinmann, M., Jutzi, B. & Mallet, C., 2014: Semantic 3D scene interpretation: A framework combining optimal neighborhood size selection with relevant features. – ISPRS Annals of the Photogrammetry, Remote Sensing and Spatial Information Sciences **II-3:** 181–188.

2. Preis: Sabine Horvath, Wien, Österreich

Integration of Relative and Global Orientation Methods using a Moving ToF Camera

Introduction

In order to reconstruct an object recorded from multiple views, the camera pose has to be known for each image. The quality of the model certainly depends on the quality of the camera orientation. For that reason this contribution deals with the estimation and enhancement of the trajectory formed by a moving Time-of-Flight (ToF) camera.

Method

The camera poses are estimated by means of the global orientation method – the bundle adjustment – on the one hand and by the relative orientation method, which bases on the range and optical flow in the image of Ghuffar et al. (2013), on the other hand. The bundle adjustment based on image observations of control points produces unbiased, but noisy estimates (Fig. 1, blue graph – Img). In contrast, the summed up relative orientations show a smooth trajectory with a large accumulated error (Fig. 1, green graph – ROF). These contrary method properties led to the formulation of the hypothesis that the integration of the two methods results in a smooth unbiased estimate of the true trajectory.

The bundle adjustment is an easily adaptable method, which simultaneously estimates all unknown parameters. Thus, the relative orientations are included in this established adjustment of indirect observations. Due to the already estimated covariance matrices of the relative orientations, the simple approach of integrating the relative orientation results has been applied. In Horvath (2014) the functional relation between the relative orientation results and the unknowns of the bundle adjustment is presented.

Another enhancement is realized by introducing the range measurements to the control points, performed by the ToF camera. The appropriate integration of these observations – image (Img), relative orientation based on the range and optical flow (ROF) and range (R) – with different precisions is computed in the course of variance component estimation.

The approach is verified on data, captured in the existing measuring field in the laboratory of the Department of Geodesy and Geoinformation. The ToF camera has been mounted on a rail-movable platform and moved linearly approximately 60 cm in horizontal direction.

First, the image observations of the bundle adjustment and the relative orientations are the only two observation groups considered. The computed trajectory, shown in Fig. 1 (Img+ROF), confirms the formulated hypothesis – the estimation much better corresponds to the true movement of the ToF camera. Furthermore, the integration improved the precision of the trajectory by a factor of 3. The calculated variance components of the relative orientations show, that these were estimated too optimistic by a factor of approximately 30. The reasons are the artificially high redundancy of the relative orientation adjustment system and not considered correlations in amplitude and range between neighbouring pixels.

Secondly, the adjustment model is extended by the range observations to the control points. The estimated trajectory is represented by the violet graph (Img+ROF+R) in Fig. 1. Due to not considered systematic range errors, the observations got deformed and the camera trajectory is moved towards the object recorded. Systematic range errors have been modelled with respect to the ranges, the amplitudes, the integration time and the position in the image according to Karel & Niedermayr (2010).

However, systematic range errors due to internal scattering and multipath effects in object space have not been considered at all.

References

Ghuffar, S., Ressl, C. & Pfeifer, N., 2013: Relative Orientation of videos from range imaging cameras. – SPIE 8791, Videometrics, Range Imaging, and Applications XII, and Automated Visual Inspection, 879114.

Horvath, S., 2014: Integration of relative and global orientation methods using a moving ToF camera. – Diploma Thesis (unpublished), TU Wien, Department of Geodesy and Geoinformation, Österreich.

Karel, W. & Niedermayr, S., 2010: Photogrammetrie + Laserscanning = range imaging. – VGI **98** (2):1–8.

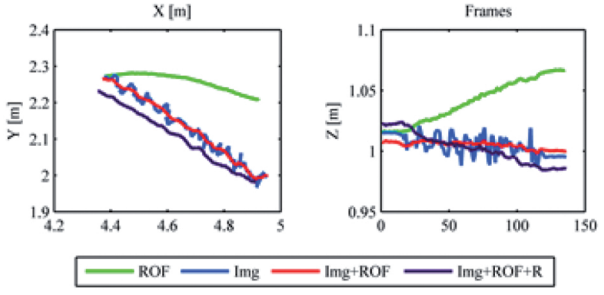

Fig. 1: Estimated camera trajectory in the global coordinate system, left: the object recorded is placed in Y = 0, right: The horizontal recording direction (*Z*-axis) in the temporal sequence (Frames) is shown.

3. Preis: Marianne Deuber, Muttenz, Schweiz

Dense Image Matching mit Schrägluftbildern der Leica RCD30 Oblique Penta

Einleitung

Bisher wurden Dense Image Matching (DIM-) Algorithmen überwiegend auf Nahbereichsaufnahmen, Nadir-Luftbilder oder im Bereich Mobile Mapping auf horizontale Bilder angewandt. Systematische Vergleiche von DIM-Algorithmen unter Verwendung von Schrägluftbildern fehlten bis anhin. In diesem Beitrag wird eine neu entwickelte Untersuchungssystematik für den Vergleich von DIM-Algorithmen vorgestellt, welche mit ausgewählten Softwareprodukten validiert wurde.

Grundlagedaten und Untersuchungssystematik

Als Grundlagedaten für die Entwicklung und die Validierung der Untersuchungssystematik dienten orientierte Luftbilder der Stadt Zürich, aufgenommen mit der Leica RCD30 Oblique Penta. Als Referenzdaten wurden ADS100 Daten, Punktwolken einer Mobile Mapping Kampagne und Punktwolken von terrestrischem Laserscanning verwendet.

Die Untersuchungssystematik ist neben Nadir- auch für Schrägluftbilder geeignet und umfasst verschiedene reproduzierbare Untersuchungen im 3D-Objekt- sowie im 2D-Bildraum. Für die Aufbereitung der Daten und die Vergleiche der DIM-Algorithmen wurde eine Vielzahl von Applikationen entwickelt.

Die konzipierten Untersuchungen lassen sich wie folgt strukturieren:

Untersuchungen im 2D-Bildraum
- Vollständigkeit von Tiefenkarten
- Differenzen von Tiefenkarten und Referenz-Tiefenwerten

Untersuchungen im 3D-Objektraum
- Dichte der Punktwolken
- Profile in den Punktwolken
- Streuung der Punktwolken
- Differenzen von Strecken in den Punktwolken
- Differenzen von absoluten 3D-Punkt-Koordinaten

Allgemeine Untersuchungen
- Prozessierungszeiten
- Limitierungen der Algorithmen

Validierung der Systematik

Die Untersuchungssystematik wurde mittels folgender Softwareprodukte validiert. Sie basieren größtenteils auf dem von Hirschmüller (2008) entwickelten Semi-Global Matching Algorithmus oder auf Abwandlungen davon.
- Agisoft PhotoScan
- Leica Xpro SGM

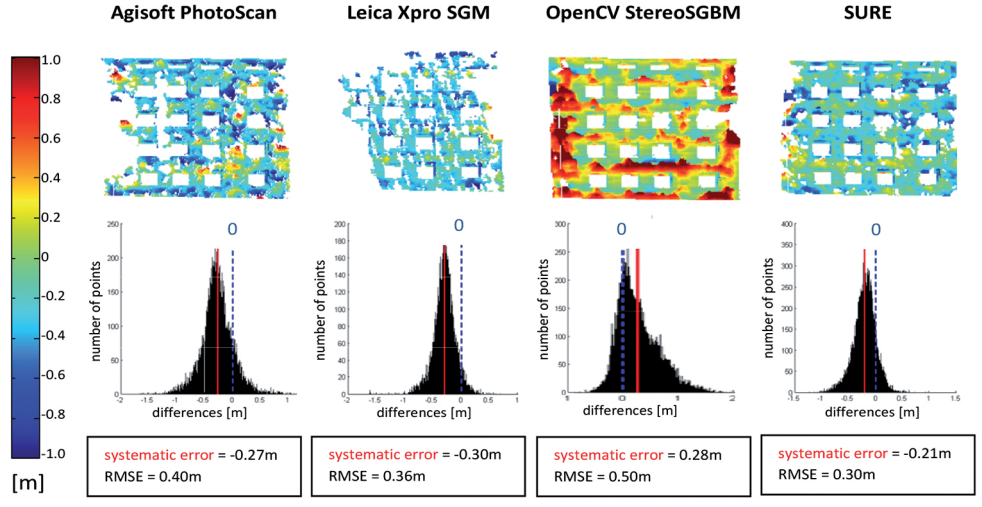

Abb. 1: Vergleich von Tiefenwerten.

- OpenCV StereoSGBM
- SURE

Nachfolgend ist ein Auszug aus den Ergebnissen aufgeführt. Die vollständigen und detaillierten Resultate sind in Deuber (2014) präsentiert.

In der Abb. 1 sind die Differenzen von generierten Tiefenkarten zu Referenztiefenwerten als Differenzbilder und Fehlerdiagramme aufgeführt. Die RMS-Werte betragen zwischen 0.3 m und 0.5 m und die Mittelwerte zwischen -0.30 m bis 0.28 m.

Fazit, Referenzen und Ausblick

Die Untersuchungssystematik ermöglicht es, Dense Image Matching Algorithmen objektiv zu beurteilen. Sie ist für Nadir- wie auch für Schrägluftbilder geeignet und unabhängig von bestimmten Kamerasystemen und Softwareprodukten. Sie kann als Grundlage für Benchmarks im Bereich Matching mit Oblique-Luftbildern verwendet werden. So enthält beispielsweise der ISPRS/EuroSDR-Benchmark (Cavegn et al. 2014) verschiedene Ansätze aus diesen Untersuchungen.

Cavegn, S., Haala, N., Nebiker, S., Rothermel, M. & Tutzauer, P., 2014. Benchmarking High Density Image Matching for Oblique Airborne Imagery. – ISPRS - International Archives of the Photogrammetry, Remote Sensing and Spatial Information Sciences, Copernicus Publications **XL-3:** 45–52, Zürich, Schweiz.

Deuber, M., 2014: Oblique Photogrammetry – Dense Image Matching mit Schrägluftbildern. – Master Thesis, Fachhochschule Nordwestschweiz, Muttenz, Schweiz.

Hirschmüller, H., 2008: Stereo Processing by Semiglobal Matching and Mutual Information. – IEEE Transactions on Pattern Analysis and Machine Intelligence **30** (2): 328–341.

Adressen der Preisträger und Betreuer:

Corinne Stucker, ETH Zürich, Tel.: +41-44-633-30-63, e-mail: stuckerc@student.ethz.ch, Betreuer: Jan Dirk Wegner, Zürich, Schweiz.

Sabine Horvath, TU Wien, Department of Geodesy and Geoinformation, A-1040 Wien, Tel.: +43-1-58801-12837, e-mail: sabine.horvath@geo.tuwien.ac.at, Betreuer: Norbert Pfeifer, Wien, Österreich.

Marianne Deuber, Fachhochschule Nordwestschweiz, Tel.: +41-44-206-1133, e-mail: marianne_deuber@hotmail.com, Betreuer: Stephan Nebiker, Muttenz, Schweiz

Mitteilung der ISPRS

Brasilianischer Verdienstorden für Prof. Christian Heipke

Prof. Christian Heipke, Leibniz Universität Hannover, wurde am 06.05.2015 in Rio de Janeiro vom Präsidenten der Brasilianischen Gesellschaft für Kartographie, Geodäsie, Photogrammetrie und Fernerkundung, Paolo Cesar T. Trino, für seine Beiträge zur internationalen Zusammenarbeit, insbesondere mit Brasilien, mit dem Verdienstorden (Comendador) für Kartographie ausgezeichnet.

Christian Heipke, Generalsekretär der ISPRS

Neuerscheinungen

WITTE, B. & SPARLA, P. (Hrsg.) 2015: *Vermessungskunde und Grundlagen der Statistik für das Bauwesen*. Wichmann-Verlag, 338 Seiten. ISBN 978-3-87907-552-2.
Das Standardwerk für Studierende und Praktiker der Fachrichtungen Vermessungs- und Bauingenieurwesen, Architektur, Geographie und Geowissenschaften zeichnet sich durch eine klare Gliederung und eine übersichtliche und leicht verständliche Darstellung aus. Zahlreiche Abbildungen lockern den umfangreichen Stoff auf, und die praktischen Beispiele ermöglichen die eigenständige Umsetzung der Lehrinhalte.

CON TERRA (Hrsg.) 2015: *FME Desktop – Das deutsche Handbuch für Einsteiger und Anwender*. Wichmann-Verlag, 338 Seiten. ISBN 978-3-87907-591-1.
Das FME Desktop Handbuch erläutert deutschsprachigen FME Einsteigern die Grundprinzipien der Arbeit mit FME Desktop und stellt eine Ergänzung bzw. eine Alternative zum englischsprachigen Handbuch und den englischen Online-Tutorials dar. Das informative Nachschlagewerk enthält zahlreiche Praxisbeispiele, nützliche Tipps und Tricks und liefert Anregungen für weitere Einsatzfelder.
Zum Herausgeber: **con terra** mit Sitz in Münster steht für zukunftsweisende Geo-IT-Lösungen und innovative Produkte. Als Unternehmen der Esri Deutschland Group setzt con terra auf das System ArcGIS und ergänzt es bei Bedarf zielgerichtet um weitere Produkte und Technologien. Fachlich liegt der Fokus in den Märkten Versicherungen, Natur-Umwelt-Ressourcen, Telekommunikation, E-Government und Immobilien sowie bei den Themen Geodateninfrastrukturen und der Modellierung und Transformation von Geodaten.

Veranstaltungskalender

2015

3. – 4. Dezember: **3D-NordOst 2015** in **Berlin**. 3d-NordOst.de

7. – 13. Dezember: **ICCV 2015 – International Conference for Computer Vision 2015** in **Santiago,** Chile. pamitc.org/iccv15/

9. – 11. Dezember: **MMT 2015: 9th International Symposium on Mobile Mapping Technology** in **Sydney,** Australien. mmt2015.org

2016

3. – 4. Februar: **Oldenburger 3D Tage** in **Oldenburg**. jade-hs.de/fachbereiche/bauwesen-und-geoinformation/geoinformation/oldenburger-3d-tage

10. – 12. Februar: **EuroCOW 2016** in **Lausanne,** Schweiz. eurocow2016.org

20. – 22. April: **Interexpo Geo-Siberia 2016** in **Novosibirsk,** Russland. http://expo-geo.ru/event/4-Interekspo_GEO-SIBIR

9. – 13. Mai: **Living Planet Symposium 2016** in **Prag,** Tschechien. http://lps16.esa.int

6. – 9. Juni: **EUSAR 2016 – 11th European Conference on Synthetic Aperture Radar** in **Hamburg.** eusar.de

26. Juni – 1. Juli: **CVPR 2016 – International Conference on Computer Vision and Pattern Recognition 2016** in **Las Vegas,** USA. pamitc.org/cvpr16

10. – 15. Juli: **IGARSS 2016 – International Geoscience and Remote Sensing Symposium 2015** in **Peking,** China. igarss2016.org

12. – 19. Juli: **ISPRS Congress 2016** in **Prag,** Tschechien. www.isprs2016-prague.com

14. – 16. September: **GEOBIA 2016** in **Enschede,** Niederlande. geobia2016.com

25. – 28. September: **ICIP 2016 – International Conference on Image Processing 2016** in **Phoenix,** USA. ieeeicip2016.org

10. – 16. Oktober: **ECCV 2016 – European Conference on Computer Vision 2016** in **Amsterdam,** Niederlande. eccv2016.org

11. – 13. Oktober: **Intergeo 2016** in **Hamburg,** Niederlande. intergeo.de

8. – 11. November: **ICPR 2016 – International Conference on Pattern Recognition 2016** in **Cancun,** Mexiko. icpr2016.org

Weitere Konferenzen und Workshops finden sich beispielsweise unter:
isprs.org/calendar/Default.aspx
conferences.visionbib.com

Korporative Mitglieder

Firmen

AEROWEST GmbH
AICON 3D Systems GmbH
aphos Leipzig AG
ASTEC GEODATA GmbH
Bernhard Harzer Verlag GmbH
Black Bridge AG
Blom Deutschland GmbH
Brockmann Consult GmbH
bsf swissphoto GmbH
Büro Immekus
DB Netz AG
DELPHI IMM GmbH
Deutsches Bergbau-Museum
EFTAS Fernerkundung Technologietransfer GmbH
ESG Elektroniksystem- und Logistik-GmbH
Esri Deutschland GmbH
EUROPEAN SPACE IMAGING
Eurosense GmbH
Exelis Visual Information Solutions GmbH
fokus GmbH
GAF GmbH
GeoCart Herten GmbH
Geoinform. & Photogr. Engin. Dr. Kruck & Co. GbR
geoplana Ingenieurgesellschaft mbH
GEOSYSTEMS GmbH
GGS - Büro für Geotechnik, Geoinformatik, Service
Hansa Luftbild AG
Herbert Wichmann, VDE Verlag GmbH
IAGB mbH
IGI - Ingenieur-Gesellschaft für Interfaces mbH
ILV-Fernerkundungs GmbH
Infoterra GmbH
INVERS - Industrievermessung & Systeme
Leica Geosystems GmbH
Linsinger ZT GmbH
Luftbilddatenbank Dr. Carls GmbH
map/x/tek
Messbildstelle GmbH
Microsoft Photogrammetry
MILAN Geoservice GmbH
M.O.S.S. Computer Grafik Systeme GmbH
PHOENICS GmbH
PMS - Photo Mess Systeme AG
RIEGL Laser Measurement Systems GmbH
RWE Power AG, Geobasisdaten/Markscheidewesen
technet GmbH
Terra-Messflug GmbH
topometric GmbH
TRIGIS GmbH
Trimble Germany GmbH
trimetric 3D Service GmbH
Z/I Imaging Ltd.

Behörden

Bayerische Landesanstalt für Wald und Forstwirtschaft
Bundesamt für Kartographie und Geodäsie
Bundesmininisterium für Ernährung, Landwirtschaft und Verbraucherschutz
Hessisches LA für Bodenmanagement und Geoinformation
Innenministerium NRW, Gruppe Vermessungswesen
Institut für Umwelt- und Zukunftsforschung
LA für Geoinformation und Landentwicklung, BW
LA für Vermessung und Geoinformation, Bayern
LA für Vermessung und Geoinformation, Schleswig-Holstein
LB Geoinformation und Vermessung, Hamburg
LB für Küstenschutz, Nationalpark und Meeresschutz, SH
Landeshauptstadt Düsseldorf, Vermessungs- und Liegenschaftsamt
Landesvermessung und Geobasisinformation Niedersachsen
Märkischer Kreis, Vermessungs- und Katasteramt
Regierungspräsident Tübingen, Abt. 8 Forstdirektion
Regionalverband Ruhr
Staatsbetrieb Sachsenforst
Stadt Köln, Amt für Liegenschaften, Vermessung und Kataster
Stadt Wuppertal, Vermessung, Katasteramt und Geodaten
Thüringer LA für Vermessung und Geoinformation
Zentrum für Geoinformationswesen der Bundeswehr

Hochschulen

BTU Cottbus, Lehrstuhl für Vermessungskunde
FH Frankfurt a.M., FB 1, Studiengang Geoinformation
FH Mainz, Institut für Raumbezogene Informations- und Messtechnik
HCU HafenCity Universität Hamburg, Geomatik
HfT Stuttgart, Vermessung und Geoinformatik
HS Bochum, FB Vermessung und Geoinformatik
HS Karlsruhe, Fakultät für Geomatik
HTW Dresden, FB Vermessungswesen/Kartographie
Jade Hochschule, Institut für Angewandte Photogrammetrie und Geoinformatik
LUH Hannover, Institut für Kartographie und Geoinformatik
LUH Hannover, Institut für Photogrammetrie und Geoinformation
MLU Halle, FG Geofernerkundung
Rhein Ahr Campus, Anwendungszentrum für multimodale und luftgestützte Sensorik
Ruhr-Uni Bochum, Geographisches Institut
RWTH Aachen, Geodätisches Institut
TU Bergak. Freiberg, Institut für Markscheidewesen und Geodäsie
TU Berlin, Computer Vision & Remote Sensing
TU Berlin, Institut für Geodäsie und Geoinformationstechnik
TU Braunschweig, Institut für Geodäsie und Photogr.
TU Clausthal, Institut für Geotechnik und Markscheidewesen
TU Darmstadt, Institut für Geodäsie, FG Fernerkundung und Bildanalyse
TU Dresden, Institut für Photogrammetrie und Fernerkundung
TU München, FG Photogrammetrie und Fernerkundung
TU München, Lehrstuhl für Geoinformatik
TU Wien, FG Photogrammetrie und Fernerkundung
Uni Bonn, Institut für Photogrammetrie
Uni Göttingen, Abt. Waldinventur und Fernerkundung
Uni Heidelberg, IWR Interdisziplinäres Zentrum für Wissenschaftliches Rechnen
Uni Kassel, FG Grünlandwissenschaften und Rohstoffe
Uni Kiel, Geographisches Institut
Uni Stuttgart, Institut für Photogrammetrie
Uni Trier, Institut für Umweltfernerkundung und Geoinformatik
Uni Würzburg, Geographisches Institut
Uni zu Köln, Geographisches Institut

Jahresübersicht 2015

Vorstand der DGPF

Präsident
Prof. Dr. rer. nat. Thomas H. Kolbe
Technische Universität München
Institut für Geodäsie, GIS und Landmanagement
Lehrstuhl für Geoinformatik
Arcisstraße 21, 80333 München
Tel.: 089 / 289-23888
Fax: 089 / 289-22878
e-mail: thomas.kolbe@tum.de

Vizepräsident
Prof. Dr.-Ing. Uwe Stilla
Technische Universität München
Fachgebiet Photogrammetrie und Fernerkundung
Arcisstraße 21, 80333 München
Tel.: 089 / 289-22671
Fax: 089 / 289-23202
e-mail: stilla@tum.de

Sekretär
Prof. Dr.-Ing. Eberhard Gülch
Hochschule für Technik Stuttgart
Fakultät Vermessung, Mathematik und Informatik
Schellingstr. 24, 70174 Stuttgart
Tel.: 0711 / 8926-2610
Fax: 0711 / 8926-2556
e-mail: sekretaer@dgpf.de

Schatzmeister
Dr.-Ing. Herbert Krauss
Rodenkirchener Straße 47, 50997 Köln
Tel.: 02233 / 22514
Fax: 032 222 / 427178
e-mail: mh.krauss@t-online.de

Hauptschriftleiter
Prof. Dr.-Ing. Wolfgang Kresse
Hochschule Neubrandenburg
Fachbereich Landschaftswissenschaften und Geomatik
Brodaer Straße 2, 17033 Neubrandenburg
Tel.: 0395 / 5693-4106
Fax: 0395 / 5693-4999
e-mail: kresse@hs-nb.de

Beirat
Prof. Dr. Cornelia Glässer
Martin-Luther-Universität Halle-Wittenberg
Institut für Geographie
Von-Seckendorff-Platz 4, 06120 Halle
Tel.: 0345 / 55-260 20
Fax: 0345 / 55-271 68
e-mail: cornelia.glaesser@geo.uni-halle.de

Beirat
Dr. rer. nat. Klaus-Ulrich Komp
EFTAS Fernerkundung Technologietransfer GmbH
Oststraße 2-18, 48145 Münster
Tel.: 0251 / 1330-70
Fax: 0251 / 1330-733
e-mail: klaus.komp@eftas.com

Beirat
Prof. Dr.-Ing. habil. Hans-Gerd Maas
Technische Universität Dresden
Professur für Photogrammetrie
Helmholtzstraße 10, 01062 Dresden
Tel.: 0351 / 463-32859
Fax: 0351 / 463-37266
e-mail: hans-gerd.maas@tu-dresden.de

Beirat
Prof. Dr.-Ing. habil. Monika Sester
Leibniz Universität Hannover
Institut für Kartographie und Geoinformatik (ikg)
Appelstraße 9a, 30167 Hannover
Tel.: 0511 / 762-3588
Fax: 0511 / 762-2780
e-mail: monika.sester@ikg.uni-hannover.de

Beirat
Dr.-Ing. Eckhardt Seyfert
Landesvermessung und Geobasisinformation Brandenburg
Heinrich-Mann-Allee 103, 14473 Potsdam
Tel.: 0331 / 8844-506
Fax: 0331 / 8844-126
e-mail: eckhardt.seyfert@geobasis-bb.de

Ehrenmitglieder der DGPF

Prof. Dr.-Ing. Friedrich Ackermann, Stuttgart
Prof. Dr.-Ing. Wolfgang Förstner, Bonn
Prof. Dr. Gerd Hildebrandt, Freiburg
Prof. Dr.-Ing. Gottfried Konecny, Hannover
Direktor Fritz Erich Krause, Münster
Dr.-Ing. Herbert Krauss, Köln
Prof. Dr.-Ing. Klaus Szangolies, Jena

Arbeitskreise der DGPF

Aus- und Weiterbildung
Prof. Dr.-Ing. Ansgar Brunn
Hochschule für angewandte Wissenschaften Würzburg-Schweinfurt
Studiengang Vermessung und Geoinformatik
Röntgenring 8, 97070 Würzburg
Tel.: 0931 / 3511-8212
Fax: 0931 / 3511-9510
e-mail: ansgar.brunn@fhws.de

Dr.-Ing. Görres Grenzdörffer
Universität Rostock, Agrar- und Umweltwissenschaftliche Fakultät
Professur Geodäsie und Geoinformatik
Justus-v.-Liebig-Weg 6, 18051 Rostock
Tel.: 0381 / 498-3206
Fax: 0381 / 498-3202
e-mail: goerres.grenzdoerffer@uni-rostock.de

Auswertung von Fernerkundungsdaten
Prof. Dr. Volker Hochschild
Universität Tübingen
Physische Geographie und GIS
Geographisches Institut
Rümelinstraße 19 – 23, 72070 Tübingen
Tel.: 07071 / 2975316
Fax: 07071 / 295378
e-mail: dgpf2013@geographie.uni-tuebingen.de

Bildanalyse und Bildverstehen
Dr.-Ing. Uwe Weidner
Karlsruher Institut für Technologie
Institut für Photogrammetrie und Fernerkundung
Englerstraße 7, 76131 Karlsruhe
Tel.: 0721 / 608-43945
Fax: 0721 / 608-48450
e-mail: uwe.weidner@kit.edu

3D-Stadtmodelle
Dipl.-Ing. Bettina Petzold
Hessisches Landesamt für Bodenmanagement und Geoinformation Schaperstraße 16, 65195 Wiesbaden
Tel.: 0611 / 535-5372
Fax: 0611 / 535-5351
e-mail: bettina.petzold@hvbg.hessen.de
www.hvbg.hessen.de

Dipl.-Ing. Ekkehard Matthias
Freie und Hansestadt Hamburg, Landesbetrieb Geoinformation und Vermessung, Sachsenkamp 4, 20097 Hamburg
Tel.: 040 / 428-26-5750
Fax: 040 / 428-26-5966
e-mail: ekkehard.matthias@gv.hamburg.de
www.geoinfo.hamburg.de

Fernerkundung in der Geologie
Dr. Hans-Ulrich Wetzel
GeoForschungsZentrum Potsdam (GFZ)
PB 1.5, Telegrafenberg, 14473 Potsdam
Tel.: 0331 / 288-1194
Fax: 0331 / 288-1192
e-mail: wetz@gfz-potsdam.de

Geoinformatik
Prof. Dr.-Ing. Jan-Henrik Haunert
Universität Osnabrück
Institut für Geoinformatik und Fernerkundung (IGF)
Barbarastraße 22b, 49076 Osnabrück
Tel.: 0541 / 969-3964
Fax: 0541 / 969-3939
e-mail: janhhaunert@uni-osnabrueck.de

Hyperspektrale Fernerkundung
Dr.-Ing. András Jung
Universität Leipzig
Institut für Geographie, Abt. für Geoinformatik und Fernerkundung
Johannisallee 19a, 04103 Leipzig
Tel.: 0341 / 9732785
Fax: 0341 / 9738619
e-mail: andras.jung@uni-leipzig.de

Optische 3D-Messtechnik
Prof. Dipl.-Ing. Thomas Kersten
HafenCity Universität Hamburg
Labor für Photogrammetrie & Laserscanning
Hebebrandstraße 1, 22297 Hamburg
Tel.: 040 / 428-27-5343
Fax: 040 / 428-27-5359
e-mail: thomas.kersten@hcu-hamburg.de,
www.hcu-hamburg.de/geomatik/kersten

Radarfernerkundung und Flugzeuglaserscanning
Prof. Dr.-Ing. Uwe Sörgel
Technische Universität Darmstadt
Institut für Geodäsie
Fachgebiet für Fernerkundung und Bildanalyse
Petersenstraße 13, 64287 Darmstadt
e-mail: soergel@geod.tu-darmstadt.de

Recht und Geodaten
Ansprechpartnerin DGPF: Dipl.-Ing. Martina Braune
Landesvermessung und Geobasisinformation Brandenburg
Heinrich-Mann-Allee 103, 14473 Potsdam
Tel.: 0331 / 8844-330
e-mail: martina.braune@geobasis-bb.de

Leiter (DGfK): Dipl.-Ing. Dietrich Diez
Landesamt für Geoinformation und Landentwicklung Baden-Württemberg
Büchsenstraße 54, 70174 Stuttgart
Tel.: 0711 / 95980-101
e-mail: dietrich.diez@lgl.bwl.de

Sensoren und Plattformen
Prof. Dr. Norbert Haala
Universität Stuttgart
Institut für Photogrammetrie
Geschwister-Scholl-Straße 24d, 70174 Stuttgart
Tel.: 0711 / 685-83383
Fax: 0711 / 685-83297
e-mail: norbert.haala@ifp.uni-stuttgart.de

Standardisierung und Qualitätssicherung
Dipl.-Ing. Sven Baltrusch
Landesamt für Innere Verwaltung Mecklenburg-Vorpommern
Amt für Geoinformation, Vermessung und Katasterwesen
Lübecker Straße 289, 19059 Schwerin
Tel.: 0385 / 588-56322
e-mail: sven.baltrusch@laiv-mv.de

Berichterstatter für ISPRS und CIPA

Kommission I – Image Data Acquisition - Sensors and Platforms
Dr.-Ing. Franz Kurz
D-82230 Oberpfaffenhofen
e-mail: franz.kurz@dlr.de

Kommission II – Theory and Concepts of Spatial Information Science
Prof. Dr.-Ing. Monika Sester
D-30167 Hannover
e-mail: monika.sester@ikg.uni-hannover.de

Kommission III – Photogrammetric Computer Vision and Image Analysis
Prof. Dr.-Ing. Stefan Hinz
D-76128 Karlsruhe
e-mail: stefan.hinz@kit.edu

Kommission IV – Geodatabases and Digital Mapping
Dr.-Ing. Volker Walter
D-70174 Stuttgart
e-mail: volker.walter@ifp.uni-stuttgart.de

Kommission V – Close-Range Sensing: Analysis and Applications
Dr.-Ing. Danilo Schneider
D-01062 Dresden
e-mail: danilo.schneider@tu-dresden.de

Kommission VI – Education and Outreach
Dipl.-Inf. Gert König
D-10623 Berlin
e-mail: gerhard.koenig@tu-berlin.de

Kommission VII – Thematic Processing, Modeling and Analysis of Remotely Sensed Data
Dr.-Ing. Uwe Weidner
D-76128 Karlsruhe
e-mail: weidner@ipf.uni-karlsruhe.de

Kommission VIII – Remote Sensing Applications and Policies

Prof. Dr. Irmgard Niemeyer
D-52425 Jülich
e-mail: i.niemeyer@fz-juelich.de

CIPA – Internationales Komitee für Architekturphotogrammetrie
Prof. Dr.-Ing. Michael Scherer
D-44780 Bochum
e-mail: michael.scherer@ruhr-uni-bochum.de

Gutachter der PFG im Jahr 2015

Die Schriftleitung dankt allen Gutachtern des Jahres 2015 für die großartige Unterstützung unserer Zeitschrift!

- Bashar Alsadik, Enschede, Niederlande
- Clement Atzberger, Wien, Österreich
- David Belton, Perth, Australia
- Erik Borg, Neustrelitz
- Oliver Buck, Münster
- Dimitri Bulatov, Ettlingen
- Dirk Burghardt, Berlin
- Volker Coors, Stuttgart
- Ana Djuricic, Wien, Österreich
- Ben Gorte, Delft, Niederlande
- Richard Gürcke, Hannover
- Stephane Guillaso, Berlin
- Klaus Hanke, Innsbruck, Österreich
- Jan-Henrik Haunert, Osnabrück
- Ludwig Högner, München
- Karsten Jacobsen, Hannover
- Carsten Jürgens, Bochum
- Boris Jutzi, Karlsruhe
- Pierre Karrasch, Dresden
- Thomas Kersten, Hamburg
- Birgit Kleinschmit, Berlin
- Patrick Knöfel, Würzburg
- Gabriela Lenzano, Mendoza, Argentinien
- José Luis Lerma Garcia, Valencia, Spanien
- Roland Linck, Kühbach
- Keng-Hao Liu, Kaoshiung, Taiwan
- Fabian Löw, Würzburg
- Thomas Luhmann, Oldenburg
- Stephan Mäs, Dresden
- Clement Mallet, Paris, Frankreich
- Gottfried Mandlburger, Wien, Österreich
- Ulrich Michel, Heidelberg
- Domen Mongus, Maribor, Slowenien
- Jens-André Paffenholz, Hannover
- Norbert Pfeifer, Wien, Österreich
- Martin Rehak, Zürich, Schweiz
- Mathias Rothermel, Stuttgart
- Ewelina Rupnik, Trento, Italien
- Michael Schmitt, München
- Johannes Schneider, Bonn
- Jan Skaloud, Lausanne, Schweiz
- Christian Strobl, Oberpfaffenhofen
- Barbara Theilen-Willige, Stockach
- Pascal Theiler, Zürich, Schweiz
- Nguyen Xuan Thinh, Dortmund
- Charles Toth, Columbus, Ohio, USA
- Tobias Ullmann, Würzburg
- Thomas Vögtle, Karlsruhe
- Jan Wegner, Zürich, Schweiz
- Andreas Wytzisk, Bochum
- Wei Yao, München

PFG – Jahrgang 2015, Heft 1 – 6
Inhaltsverzeichnis Jahrgang 2015

Editorial

Originalbeiträge

 www.schweizerbart.de
DOI: 10.1127/1432-8364/2015/0282 1432-8364/15/0282 $ 0.00

Beiträge aus Wissenschaft und Praxis

Berichte und Mitteilungen